


An Amphibole Perspective on the Recent Magmatic Evolution of Mount St. Helens

Franziska Keller¹ ^{1,2,3,*}, Maren Wanke⁴, Nico Kueter⁵, Marcel Guillong¹ and Olivier Bachmann¹

¹Department of Earth Sciences, Institute of Geochemistry and Petrology, ETH Zürich, Clausiusstrasse 25, 8092 Zürich, Switzerland

²Department of Earth Sciences, University of Oregon, 100 Cascade Hall, 1272 Eugene, OR 97403, USA

³Department of Earth and Environmental Sciences, Lehigh University, STEPS Building, 1 West Packer Ave, Bethlehem 18015, PA, USA

⁴GEOMAR Helmholtz Centre for Ocean Research Kiel, Wischhofstr. 1-3, 24148 Kiel, Germany

⁵Department of Earth Sciences, Geological Institute, ETH Zürich, Sonneggstrasse 5, 8092 Zürich, Switzerland

*Corresponding author. Telephone: +49 1522 8501965. E-mail: frk323@lehigh.edu

Compositional variations of amphibole stratigraphically recovered from multiple eruptions at a given volcano have a great potential to archive long-term magmatic processes in its crustal plumbing system. Calcic amphibole is a ubiquitous yet chemically and texturally diverse mineral at Mount St. Helens (MSH), where it occurs in dacites and in co-magmatic enclaves throughout the Spirit Lake stage (last ~4000 years of eruptive history). It forms three populations with distinct geochemical trends in key major and trace elements, which are subdivided into a high-Al (11–14.5 wt% Al₂O₃), a medium-Al (10–12.5 wt% Al₂O₃), and a low-Al (7.5–10 wt% Al₂O₃) amphibole population.

The oldest investigated tephra record (Smith Creek period, 3900–3300 years BP) yields a bimodal amphibole distribution in which lower-crustal, high-Al amphibole cores (crystallized dominantly from basaltic andesite to andesite melts) and upper-crustal, low-Al amphibole rims (crystallized from rhyolitic melt) document occasional recharge of a shallow silicic mush by a more mafic melt from a lower-crustal reservoir. The sudden appearance of medium-Al amphiboles enriched in incompatible trace elements in eruptive periods younger than 2900 years BP is associated with a change in reservoir conditions toward hotter and drier magmas, which indicates recharge of the shallow silicic reservoir by basaltic melt enriched in incompatible elements. Deep-crystallizing, high-Al amphibole, however, appears mostly unaffected by such incompatible-element-enriched basaltic recharge, suggesting that these basalts bypass the lower crustal reservoir. This could be the result of the eastward offset position of the lower crustal reservoir relative to the upper crustal storage zone underneath the MSH edifice. Amphibole has proven to be a sensitive geochemical archive for uncovering storage conditions of magmas at MSH. In agreement with geophysical observations, storage and differentiation have occurred in two main zones: an upper crustal and lower crustal reservoir (the lower one being chemically less evolved). The upper crustal silicic reservoir, offset to the west of the lower crustal reservoir, has captured compositionally unusual mafic recharge (drier, hotter, and enriched in incompatible trace elements in comparison to the typical parental magmas in the region), resulting in an increased chemical diversity of amphiboles and their carrier intermediate magmas, in the last ~3000 years of MSH's volcanic record.

Key words: amphibole; fractional crystallization; magmatic plumbing system; Mount St. Helens; volcanic evolution

INTRODUCTION

Amphibole is a key mineral in subduction zone magmas, where it plays an important role in the hydrous differentiation of calc-alkaline melts, and thus, significantly contributes to the generation of new continental crust. It typically occurs in andesitic to dacitic arc volcanoes (see compilations in Kent, 2014; Putirka, 2016; Ridolfi et al., 2010), and if lacking as a phenocryst phase in volcanic units, cryptic crystallization of amphibole has been recognized from magma chemistry at mid to lower crustal depths (e.g. Davidson et al., 2007). The importance of deep amphibole crystallization on magmatic differentiation and crustal evolution is also confirmed by petrologic experiments (Sisson et al., 2005; Alonso-Perez et al., 2009; Müntener & Ulmer, 2018), by amphibole cumulate fragments delivered from depth (Arculus & Wills, 1980; Smith, 2014; Klaver et al., 2017), and by studies on exposed lower crustal arc sections such as the Chelan Complex (Dessimoz et al., 2012), the Faminian arc (Walker et al., 2015), and the Kohistan arc (Jagoutz, 2010).

Due to its wide stability range, amphibole has great potential for archiving magmatic processes (e.g. Rutherford & Devine, 2003; Humphreys et al., 2006; Dessimoz et al., 2012; De Angelis et al., 2013; Kent, 2014; Kiss et al., 2014), where its chemistry readily adapts to changes in temperature, pressure, redox state, melt composition, and co-existing mineral or volatile phases (e.g. Hammarstrom & Zen, 1986; Hollister et al., 1987; Holland & Blundy, 1994; Anderson & Smith, 1995; Bachmann & Dungan, 2002; Ridolfi et al., 2010; Putirka, 2016; Higgins et al., 2022). Changes in any of these parameters may then be preserved within the amphibole as compositional zonation, resorption, breakdown, or entrapment of mineral or melt inclusions. Previous studies furthermore emphasize the dominant effect of melt composition on the amphibole chemistry (Erdmann et al., 2014; Putirka, 2016; Zhang et al., 2017), which can be used to calculate equilibrium melt compositions of amphibole (Zhang et al., 2017; Humphreys et al., 2019; Higgins et al., 2022).

Mount St. Helens (MSH) volcano in the southern Washington Cascades possesses a ~270 kyrs-long history of intermittent

Received: June 18, 2023. Revised: October 31, 2023. Accepted: December 4, 2023

© The Author(s) 2024. Published by Oxford University Press.

This is an Open Access article distributed under the terms of the Creative Commons Attribution License (<https://creativecommons.org/licenses/by/4.0/>), which permits unrestricted reuse, distribution, and reproduction in any medium, provided the original work is properly cited.

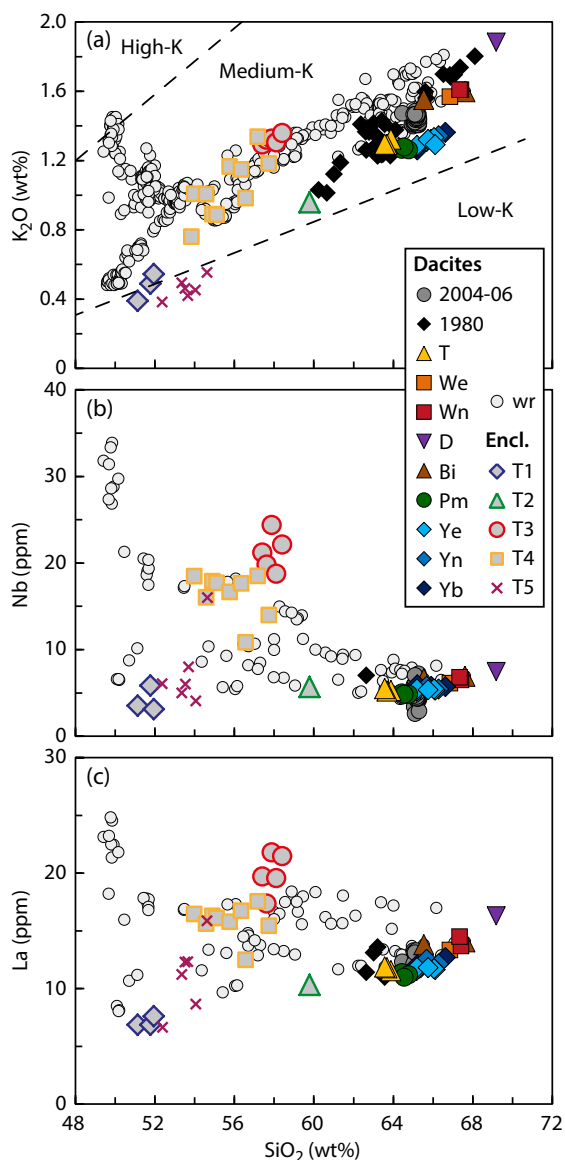


Fig. 1. Compositions of volcanic rocks and mafic enclaves (Encl.) from MSH. Enclaves (types 1–5) measured in this study are displayed as gray symbols with thick colored rims, while data for major dacitic tephra layers discussed in this study are taken from Wanke et al. (2019b) and are shown as colored symbols of variable shape. (a) K_2O vs. SiO_2 , (b) Nb vs. SiO_2 , and (c) La vs. SiO_2 . Fields for high-K, medium-K, and low-K series in (a) are drawn after Gill (1981). Whole rock (wr) compositions from literature are taken from Halliday et al. (1983), Melson (1983), Sama-Wojcicki et al. (1981), Smith & Leeman (1987), Wanke et al. (2019a), and Wanke et al. (2019b) to reference the full compositional variability of products erupted at MSH. 1σ errors of the measured elements are smaller than the plotted symbol size.

eruptions of amphibole-bearing tephra (Mullineaux, 1996; Clynne et al., 2008). Even though its eruptive products span the compositional range from basalt to rhyodacite (Fig. 1), dacite represents by far the most abundant rock type at MSH (>90%, Hildreth, 2007). Amphiboles in the most recent eruptions of MSH (1980–2008) similarly show a continuous compositional spectrum with a peak at intermediate Al_2O_3 contents between 10 and 12.5 wt% (Thorner et al., 2008; Humphreys et al., 2019), which is in contrast to many other intermediate arc volcanoes that typically record bimodal amphibole populations (e.g. compilation in Kent, 2014). This divergence has led to a number of speculations

concerning the magmatic plumbing system of MSH and has, to date, been primarily attributed to the great vertical extension of the upper crustal part of the system, producing continuous amphibole compositions over wide pressure ranges (Pallister et al., 2008; Rutherford & Devine, 2008; Ridolfi et al., 2010; Turner et al., 2013). However, in a previous study, we reported bimodal distributions of amphibole compositions in early dacites of the Smith Creek period (Yn and Ye units, Table 1), which erupted ~3350 years ago (Wanke et al., 2019b). This change from bimodal to continuous amphibole compositions in the MSH dacites implies significant changes in the magmatic plumbing system over the last few thousand years. At the same time, dacites report pronounced variations in pre-eruptive temperature, oxygen fugacity, and water content (Smith & Leeman, 1987; Gardner et al., 1995a; Gardner et al., 1995c), which should also be recorded by amphibole phenocrysts.



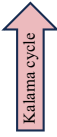
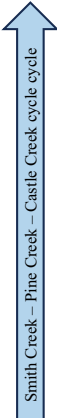
Several studies addressed amphibole composition and stability in 1980–1986 (Rutherford & Devine, 1988; Rutherford & Hill, 1993; Humphreys et al., 2019) and 2004–2006 dacites (Rutherford & Devine, 2008; Thorner et al., 2008), yet a comprehensive investigation of the amphibole assemblage over time is lacking. In aiming to unravel the geologically recent magmatic history of MSH, we have characterized and interpreted compositions and textures of the amphibole population in 11 major dacitic tephra layers of MSH deposited over the past 3900 years. The tephra record is complemented by co-magmatic, amphibole-bearing enclaves (previously referred to as co-magmatic inclusions, Heliker, 1995). Following a study on 1980 amphiboles by Humphreys et al. (2019), we particularly aim to determine the diversity of melt compositions beneath the volcano, focusing on temporal changes.

ERUPTIVE CYCLES AND PETROLOGICAL BACKGROUND

The eruptive history of MSH was first established by Crandell and Mullineaux (Mullineaux & Crandell, 1981; Mullineaux, 1986; Crandell, 1987) and was recently refined by mapping and age dating by Wolfe and Clynne (compiled in Clynne et al., 2008; Pallister et al., 2017). MSH's eruptive history is defined by four eruptive stages separated by several thousand years of dormancy: Ape Canyon (>270–35 ka), Cougar (28–18 ka), Swift Creek (16–10 ka), and Spirit Lake (3900 years BP). The youngest stage, Spirit Lake, has been further subdivided into seven eruptive periods interrupted by several hundred years of repose intervals. Each eruptive period is characterized by at least one major set of tephra deposits (Table 1). Hopson & Melson (1990) describe cyclic eruption patterns that comprise a progression from Plinian eruptions to dome growth accompanied by pyroclastic flows and tephra, and in some cases, lava flows and pyroclastic outbursts. These cycles also show a progression toward more mafic whole rock compositions and mineral assemblages, in which orthopyroxene replaces cummingtonite, while calcic amphibole diminishes and disappears and augite and olivine appear. Four of these cycles are observed during the Spirit Lake stage: the Smith Creek-Pine Creek-Castle Creek cycle, Kalama cycle, Goat Rocks cycle, and the current modern cycle (Table 1; Hopson & Melson, 1990; Pallister et al., 1992).

Mafic magmas from MSH show striking petrological diversity. The eruption of basalt is restricted to the end of the Castle Creek period (2025–1700 years BP), when three different mafic endmembers erupted in close spatial and temporal succession: (1) high-field-strength element (HFSE)-rich basalts enriched in most incompatible elements, (2) low-K olivine tholeiites (LKOT)

Table 1: Distribution of amphibole types in major dacitic tephra units and co-magmatic enclaves from MSH during the Spirit Lake stage

Eruption cycle ¹	Eruptive period	Symbol	Unit	Age ²	Amphibole types		
					Low-Al ₂ O ₃ MgHbl	Medium-Al ₂ O ₃ MgHst/Tsch	High-Al ₂ O ₃ MgHst/Tsch
	Modern 1980–2008 CE	◆	Ash set 1980	1980	++	++	++
	Goat Rocks period 1800–1857 CE	▲	T	1800 CE	(+)	+	+
	Kalama period 1479–1750 CE	■	Type 4	Early Kalama	–	++	–
		■	We	1482 CE	(+)	+	+
	Sugar Bowl period 1050–1000 years BP	■	Wn	1479 CE	++	++	+
		▼	D	1030 years BP	–	++	–
	Castle Creek period 2025–1700 years BP	▲	Bi	1990 years BP	+	(+)	+
	Pine Creek period 3000–2550 years BP	●	Pu	2670 years BP	++	(+)	++
		○	Type 3	Early Pine Creek	–	++	–
		▲	Type 2	Early Pine Creek	–	++	–
		◆	Type 1	Early Pine Creek	++	–	++
		●	Ps	2800 years BP	++	(+)	++
		●	Pm	2900 years BP	++	(+)	++
	Smith Creek period 3900–3300 BP	◆	Ye	3315 years BP	++	–	++
		◆	Yn	3350 years BP	++	–	++
◆		Yb	3900 years BP	(+)	–	++	

++, abundant; +, present; (+), rare; –, not recognized

¹Eruption cycles according to Hopson & Melson (1990) and Pallister et al. (1992); M, Modern cycle, G, Goat Rocks cycle

²Ages from Clyne et al. (2008) and Pallister et al. (2017). Dashed Pine Creek ages are estimated based on stratigraphic position.

with comparably low abundances of incompatible trace elements, and (3) arc-type basaltic andesites with a typical subduction zone signature (Fig. 1; Leeman & Smith, 2018; Smith & Leeman, 1993; Wanke et al., 2019a). This diversity is interpreted to reflect different mantle sources and melting processes, including relatively dry decompression melting (Leeman et al., 1990; Leeman & Smith, 2018; Wanke et al., 2019a) and flux melting in the mantle (Wanke et al., 2019a). MSH andesites are mostly interpreted as mixing products between HFSE-rich basalts and dacite (Pallister et al., 1992; Smith & Leeman, 1993).

In contrast to the basalts, MSH dacites appear relatively uniform despite their high abundance. They are usually crystal-rich (20–55%; Gardner et al., 1995a) and contain phenocryst assemblages of plagioclase, orthopyroxene, calcic amphibole, titanomagnetite, ilmenite, and accessory apatite and zircon in rhyolitic glass (Mullineaux, 1986; Smith & Leeman, 1987). Smith Creek tephra (Y units, Table 1), which erupted first during the Spirit Lake stage (3900 years BP - present), and some of the pre-Spirit Lake dacites, contain cummingtonite in place of orthopyroxene. In the younger dacites, minor amounts of quartz and biotite are found only in unit Yb (Smith Creek period). The most mafic dacites that erupted during the Castle Creek and Goat Rocks periods (units Bi and T) contain additional clinopyroxene.

SAMPLES AND ANALYTICAL TECHNIQUES

We report *in situ* studies on amphibole from 23 dacitic tephra samples and 15 mafic to intermediate enclaves from MSH (Suppl. Table 1) that erupted during the Spirit Lake stage (3900 years BP - present) but pre-dating the 1980 eruptions. Seventeen of the tephra samples were taken from the collection of D. Mullineaux stored at the Cascade Volcano Observatory (CVO) in Vancouver, Washington. Magmatic enclaves were collected from dacite dome rocks of Pine Creek and Kalama age pyroclastic flows. U-Pb zircon ages of magmatic enclaves were obtained by laser ablation-inductively coupled plasma-mass spectrometry (LA-ICP-MS) using the method of Guillong et al. (2014) and are reported in Supplementary Table 2.

Whole rock analyses of 30 enclaves were performed on subsamples of 50–100 g. After being crushed and pulverized, 1.5 g of rock powder was heated to 950 °C for 2 h to determine the loss on ignition (LOI). The powders were then melted down together with lithium tetraborate metaborate flux as glass beads. Major elements were measured using a PANalytical wavelength-dispersive X-ray AXIOS spectrometer at ETH Zurich (Switzerland). Relative errors are <1% for most major elements and <2% for Na₂O (Wanke et al., 2019a). Trace elements were measured by LA-ICP-MS on the fused glass beads used for XRF analyses using a Geolas

Laser Ablation System coupled with an Elan 6100 DRC (Perkin Elmer) mass spectrometer. Samples and blanks were ablated for 60 s with a 10 Hz repetition rate and a beam diameter of 90 μm (40 μm for a NIST-610 synthetic glass standard).

Drift correction and data reduction were performed using the SILLIS software (Guillong *et al.*, 2008), with Ca as an internal element standard. Results from three points were averaged for each sample. Reproducibility of a BCR-2 standard is better than 5–10% for most trace elements (Wanke *et al.*, 2019a). Whole rock compositions of tephra samples are given in Wanke *et al.* (2019b).

Mineral separates were handpicked from crushed tephra and enclave samples (except for Fe-Ti oxides, which were separated from the sample by heavy liquid separation). The minerals were then embedded in epoxy and imaged with a JEOL JSM-6390LA scanning electron microscope (SEM) at ETH Zurich (Switzerland). Major elements were analyzed by electron probe microanalysis (EPMA) using a JEOL JXA-8200 electron microprobe at ETH Zurich (Switzerland) and a JEOL JXA 8900R electron microprobe at CAU Kiel (Germany).

More than 250 amphibole phenocrysts from 38 samples were measured with an acceleration voltage of 15 keV, 15–20-nA beam current, and a focused beam. For the analysis of plagioclase rims and adjacent glass from 15 tephra samples beam currents were reduced to 10 nA and spot sizes of 5 and 10 μm , respectively, were applied. More than 250 touching magnetite-ilmenite pairs from 18 tephra samples were analyzed with 15 keV, 30 nA, and a focused beam.

Calibration parameters and all analyses of mineral phases, glass, and standard reference material are given in Supplementary Tables 4–8.

Amphibole trace elements were analyzed using a 193-nm excimer laser coupled with a second-generation two-volume constant geometry ablation cell (Resonetics: S-155LR) and a high-sensitivity sector field ICP-MS (Thermo: Element XR) at ETH Zurich. Points previously analyzed by EPMA were ablated for 40 s with a pulse rate of 10 Hz and a beam diameter of 30 μm . After every 25 analyses, a NIST-612 and a USGS GSD-1D synthetic glass standard were measured. These are then used for drift correction and data reduction using the SILLIS software (Guillong *et al.*, 2008). Concentrations were calculated using the CaO concentrations of calcic amphiboles and the SiO₂ concentration of cummingtonite previously obtained by EPMA for internal standardization. The analytical error for individual analyses is difficult to quantify, but long-term laboratory reproducibility of homogeneous glass standards yields precision well above 5% for elements with concentrations well above the detection limit. All analyses are given in Supplementary Table 4.

RESULTS

All dacitic tephra and some co-magmatic enclaves from MSH contain calcic amphiboles that encompass a variety of textures and compositions. Below, we first distinguish co-magmatic enclaves from xenolithic material. Then, we provide a detailed investigation of amphiboles in dacitic tephra layers and determine their equilibrium melts to track changes in the amphibole assemblage over time and couple these to variations in the magmatic plumbing system.

Magmatic enclaves

Classification of amphibole-bearing co-magmatic enclaves

Even though the presence of co-magmatic enclaves is rare in eruptive products of MSH, some enclaves of variable origin have

been recovered from dacite dome rocks in Spirit Lake stage pyroclastic flows (Suppl. Fig. 1). Enclaves containing amphibole could be subdivided into five distinct types (of which types 1, 2, and 3 were sampled from Pine Creek age dacite, while type 4 enclaves were taken from Kalama age dacite; for detailed descriptions, see Wanke, 2019):

- Type 1: Hornblende-gabbro with a mineral assemblage dominated by amphibole and plagioclase and minor amounts of orthopyroxene, oxides, and apatite. Type 1 enclaves typically have low SiO₂ (<52 wt%) contents and low amounts of incompatible trace elements compared to MSH whole rocks (Fig. 1).
- Type 2: Coarse-grained, dioritic mush with an assemblage of plagioclase, amphibole, orthopyroxene, and oxides (and trace amounts of apatite and zircon). Typical whole rock compositions are ~60 wt% SiO₂. Trace element concentrations are low.
- Type 3: Coarse-grained, dioritic mush with a very similar mineral assemblage and whole rock SiO₂ contents as type 2 enclaves, but showing characteristic enrichment of most incompatible elements (Nb = 18–22 ppm, La = 17–22 ppm), similar to that observed in HFSE-rich basalts from MSH (Wanke *et al.*, 2019a).
- Type 4: Quenched basaltic andesites and andesites containing an assemblage dominated by fine-grained amphibole and plagioclase with minor amounts of olivine, ortho-, and clinopyroxene, and oxides. Type 4 enclaves (54–58 wt% SiO₂) are enriched in incompatible elements but weaker than type 3 enclaves.
- Type 5: A variety of xenolithic gabbro-norites found in Castle Creek and Kalama dacites.

To distinguish coarse-grained, co-magmatic enclaves from pre-existing, xenolithic material, zircon-bearing enclaves were dated and compared to known ages of material around MSH.

U-Pb zircon ages from a type 2 (5–108 kyrs; *n* = 29) and a type 3 (45–486 kyrs; *n* = 16) enclave each fall within the age range of zircons from MSH dacites (up to 500–600 ka; Claiborne *et al.*, 2010), indicating that these represent fragments of cognate crystal mush (Suppl. Fig. 2). In contrast, zircons from a type 5 gabbro-norite enclave returned U-Pb ages of 24.9–26.3 Ma (*n* = 55) similar to zircons dated by SHRIMP from four gabbro-norite and norite enclaves (20–26 Ma, J. Pallister, pers. comm.), relating those to older crust beneath MSH. Zircon is lacking in type 1 enclaves, but similar amphibole chemistry in type 1 and 2 enclaves and Pine Creek dacite (see below) strongly indicates a co-genetic relationship. In contrast to those coarse-grained enclaves, type 4 enclaves sampled from Kalama domes are fine grained, mostly with quenched texture, and thus represent young material. A detailed description of the enclaves can be found in Wanke (2019).

Amphiboles in co-magmatic enclaves

Amphiboles in type 1 and type 2 enclaves appear strongly resorbed, mostly yielding the cores of previously larger crystals that are normally zoned with respect to Al₂O₃ (Fig. 2a and b). A distinct compositional gap between high-Al (11.7–14.6 wt% Al₂O₃) cores and low-Al (8.7–9.5 wt% Al₂O₃) rims is preserved in amphiboles of type 1 enclaves, while type 2 enclaves contain primarily high-Al amphiboles cores with decomposed rims (Figs 2b and 3c). Cores appear darker on SEM images (Fig. 2a and b) and are classified as magnesiohastingsite (MgHst) and rare tschermakite (Tsch) and pargasite (Parg), while rims classify as magnesiohornblende (MgHbl) (following the ‘average

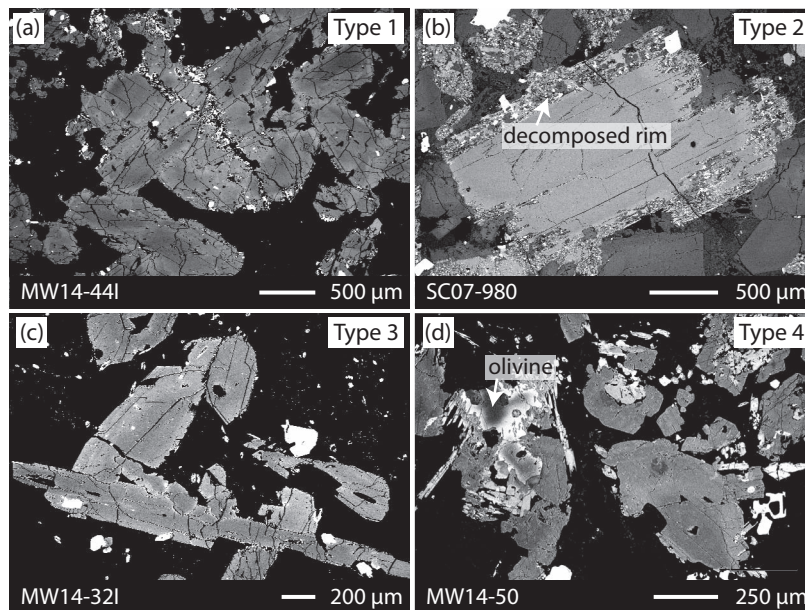


Fig. 2. Backscattered electron images of amphiboles in different types of mafic enclaves from MSH. (a) Type 1: hornblende-gabbro with normally zoned amphibole, (b) type 2: dioritic mush with decomposed amphibole, (c) type 3: dioritic mush with normally zoned amphibole, and (d) type 4: quenched basaltic andesite with amphibole crystallizing at the expense of olivine. Crystals without olivine have darker, higher-Mg cores. Type 5 enclaves are omitted in this figure due to their xenolithic origin.

Fe^{3+} method of Leake *et al.*, 1997). Core compositions of amphiboles from type 1 and type 2 enclaves overlap with respect to major and trace elements (Figs 3c and 4a).

Amphiboles in type 3 enclaves are euhedral and mostly well preserved, contrasting those in type 2 enclaves, but show similar progressive normal zoning (Fig. 2c). These amphiboles have medium-Al (9.7–12.6 wt% Al_2O_3) contents (Fig. 3c), falling in the compositional gap observed between the core and rim chemistry of amphiboles found in type 1 enclaves and are classified as MgHst/Tsch. Although Al_2O_3 concentrations partly overlap with those of high-Al MgHst/Tsch, they yield characteristically elevated TiO_2 concentrations of up to 5.1 wt% (0.55 apfu) in contrast to 1.8 to 2.7 wt% (0.3 apfu) in type 1 and 2 amphiboles; some crystal cores reach kaersutite (Kaer) compositions (Suppl. Fig. 9a).

Amphiboles in quenched type 4 mafic enclaves are compositionally similar to those in type 3 but yield an extended compositional range toward a more mafic endmember (10.3–13.4 wt% Al_2O_3 , Fig. 3b) and are significantly smaller in size (Fig. 2d). Most grains show progressive normal zoning. Amphiboles in the most mafic samples crystallize around resorbed olivine or have darker high-Mg cores (Fig. 2d). Rarely, the more evolved rims have low-Al (8.7–9.9-wt% Al_2O_3) MgHbl compositions.

Differences between amphiboles in type 1 and 2 enclaves versus type 3 and 4 enclaves are also expressed in their trace element chemistry:

- REE in amphibole in type 1 and 2 enclaves increase from MgHst/Tsch toward MgHbl (Suppl. Fig. 4) with less pronounced Eu-anomalies in MgHst/Tsch ($\text{Eu}/\text{Eu}^* = 0.9\text{--}1.1$) than in MgHbl ($\text{Eu}/\text{Eu}^* = 0.7\text{--}0.9$; Fig. 4a). Simultaneously, Sr decreases from 160–240 ppm in high-Al MgHst/Tsch to 40–130 ppm in low-Al MgHbl (Suppl. Fig. 8), accompanied by an increase in most other incompatible trace elements (Suppl. Table 4).
- Medium-Al MgHst/Tsch in type 3 and 4 enclaves generally have higher contents and larger ranges of most incompatible trace elements (REE, Nb, Zr, P, Ba, Sc, Rb) than high-Al MgHst/Tsch (Eu/Eu^* decreases from 0.9–1.1 to 0.7–0.8, Sr

from 300–400 to 150–200 ppm; Fig. 4a, Suppl. Figs 4 and 8, Suppl. Table 4). Some crystals are strongly enriched in incompatible elements (up to 40 ppm Nb and 15 ppm La), clearly exceeding trace element contents in high-Al MgHst/Tsch and MgHbl (Fig. 4a).

Type 5 Tertiary gabbronorite enclaves yield amphiboles with highly evolved MgHbl composition, which differ significantly from those in co-magmatic enclaves by higher K and REE concentrations and lower Mg# (Fig. 4a, Suppl. Table 4).

Amphiboles in dacitic tephtras

Zoning textures

In contrast to amphiboles from co-magmatic enclaves, which display predominantly normal zoning patterns, calcic amphiboles in MSH dacitic tephtras show much greater internal textural diversity. Commonly observed zoning patterns include normally zoned (with respect to Al_2O_3 , Fig. 5a and b) and patchy zoned crystals (Fig. 5c and d), as well as combinations of these referred to as multiple zoning (e.g. patchy cores overgrown by normally zoned rims, Fig. 5e–g). Besides the commonly found zoning patterns, additional cummingtonite cores overgrown by calcic amphibole rims (Fig. 5h) are found exclusively in older Smith Creek tephtras (3900–3300 years BP), which erupted first in the Spirit Lake stage after the 9000-year quiescence period.

Unzoned amphibole crystals (Fig. 5i) dominate the amphibole assemblage in the Sugar Bowl rhyodacite (unit D), but are otherwise rarely found in MSH dacite tephtras. In zones with low and medium Al_2O_3 content, inclusions of FeTi oxides and apatite are frequently found.

Most zoning patterns occur in all dacitic tephtras throughout the Spirit Lake stage. However, a shift from predominantly simple zoning patterns (i.e. mostly normal zoning) in amphiboles erupted at the beginning of the Spirit Lake stage (with exception of the first unit Yb) to increasingly more complex (i.e. mostly multiple zoning) zoning patterns in more recent eruptions can be seen.

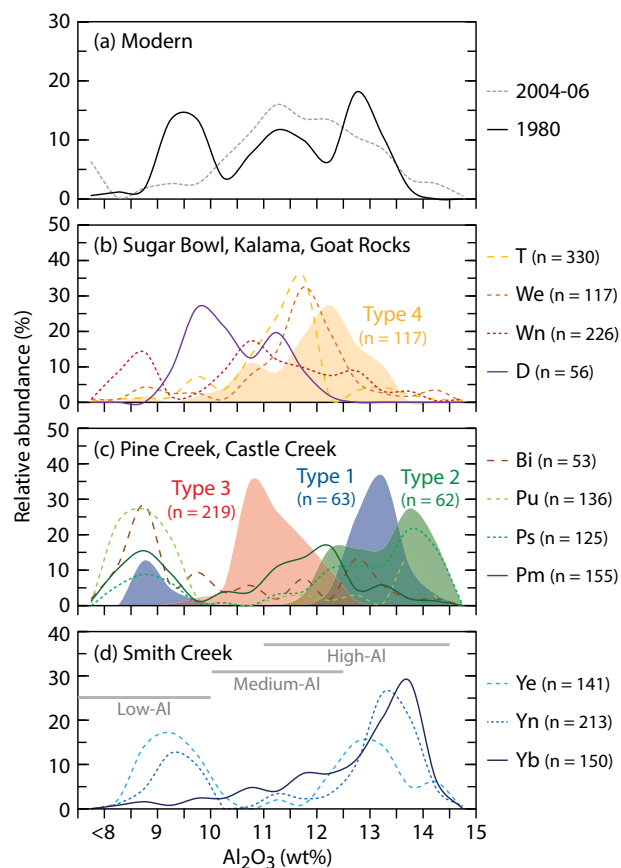


Fig. 3. Histograms of Al_2O_3 in amphiboles from dacitic tephras and mafic enclaves throughout the Spirit Lake stage indicate a trend from a bimodal distribution with high- Al_2O_3 MgHst/Tsch and low- Al_2O_3 MgHbl compositions to a continuous compositional range dominated by medium- Al_2O_3 compositions. Data for the 1980 and 2004–2006 eruptions in (a) are derived from Humphreys et al. (2019) and Thorber et al. (2008). Data from amphiboles of type 5 mafic enclaves are not included in this figure due to their xenolithic origin. (n) represents the number of all measurement points (both point as and line measurements) included from each unit.

Amphibole chemistry

Calcic amphiboles in MSH dacites cover a wide range of major ($\text{Al}_2\text{O}_3 = 7.7\text{--}14.6$ wt%, $\text{SiO}_2 = 40.3\text{--}48.1$ wt%, Fig. 3, Suppl. Table 4) and trace element compositions ($\text{Sr} = 22\text{--}298$ ppm, $\text{Nb} = 1\text{--}28$ ppm, $\text{La} = 0.6\text{--}19.3$ ppm, Fig. 4b–e, Suppl. Fig. 8). Such compositional ranges can be observed even within individual grains. Similar to the chemical diversity measured in amphiboles from co-magmatic enclaves, the amphiboles from dacitic MSH tephtras can be classified into three distinct populations: (1) a high-Al population ($11\text{--}14.5$ wt% Al_2O_3) and (2) a low-Al population ($7.5\text{--}10$ wt% Al_2O_3), which are both present in all Spirit Lake periods (except the Sugar Bowl rhyodacite) and are chemically similar to amphiboles found in type 1 and 2 co-magmatic enclaves, and (3) a medium-Al population ($10\text{--}12.5$ wt% Al_2O_3) chemically similar to amphiboles in type 3 and 4 co-magmatic enclaves, which are enriched in Ti and incompatible elements compared to high-Al amphiboles. Such medium-Al MgHst/Tsch first appears as a rare phase in tephtras from the Pine Creek period (Figs 3c and 4d), before it becomes one of the three dominant amphibole populations in younger dacites (Figs 3a and b and 4b and c).

All calcic amphiboles are enriched in middle (M) REE, typical of igneous amphibole, and show an overall increase of REE from less-evolved high-Al MgHst/Tsch toward more evolved low-Al MgHbl (Suppl. Figs 5–7). A progressive Eu depletion (from $\text{Eu}/\text{Eu}^* = 1.2\text{--}0.8$ to $0.4\text{--}0.6$; Fig. 4b–e), accompanied by a decrease in Sr (from $\text{Sr} = 200\text{--}300$ to $20\text{--}70$ ppm; Suppl. Fig. 8) and an increase in most other incompatible trace elements is observed in the dacitic MSH tephtras from high-Al MgHst/Tsch toward low-Al MgHbl, indicating the co-crystallization of plagioclase during progressive differentiation. The most mafic high-Al MgHst/Tsch overlap in composition with those in the type 1 and 2 enclaves (Fig. 4b–e). Overall, however, MgHst/Tsch in the dacites show a wider range toward more evolved compositions with higher contents of most incompatible trace elements than in the enclaves (Suppl. Figs 4–7). MgHbl in the dacites also extend to more evolved compositions and differ from those in the enclaves by a more pronounced negative Eu-anomaly.

Medium-Al MgHst/Tsch differ from the high-Al MgHst/Tsch to low-Al MgHbl trend by variable enrichment of most incompatible trace elements and by a more pronounced negative Eu-anomaly compared to high-Al MgHst/Tsch (at similar ^{14}Al , Fig. 4). Some medium-Al MgHst/Tsch are particularly enriched in incompatible trace elements (with up to 30 ppm Nb), similar to amphiboles in type 3 and 4 co-magmatic enclaves (Fig. 4).

Cummingtonite is only present in Smith Creek and some earlier dacites and has a restricted compositional range ($\text{Mg}\# = 0.6\text{--}0.7$, $\text{SiO}_2 = 51\text{--}54$ wt%). Trace element abundances are about an order of magnitude lower than in calcic amphiboles (Suppl. Fig. 5) and yield a depletion in LREE over HREE ($\text{La}/\text{Yb} = 0.04\text{--}0.29$). It has low Sr (1–5 ppm) and negative Eu-anomalies ($\text{Eu}/\text{Eu}^* = 0.3\text{--}0.7$).

Predicted melt compositions in equilibrium with amphibole

We calculated major and trace element compositions of amphibole equilibrium melts (AEMs) following the approaches from Zhang et al. (2017) and Humphreys et al. (2019). To test the reliability of the calculated AEMs, resulting AEMs from MgHbl rims of the MSH dacite tephtras were compared to measured compositions of quenched volcanic glasses surrounding these amphiboles. The wide overlap between the calculated and measured melts infers the correctness of the modeled AEM compositions, even when no quenched parental melt is available.

Calculated AEMs for amphiboles from both MSH dacites and mafic enclaves span a wide compositional range from basaltic andesite to rhyolite ($54\text{--}79$ wt% SiO_2 , Fig. 6). Silica distribution diagrams indicate that high-Al MgHst/Tsch and low-Al MgHbl found in all the dacitic tephtras and in type 1 and 2 co-magmatic enclaves grew in equilibrium with predominantly andesitic and rhyolitic melts, respectively, with a distinct compositional gap (Fig. 6). In contrast, medium-Al MgHst/Tsch occurring in Pine Creek and younger dacites, as well as in type 3 and 4 co-magmatic enclaves, yield andesitic to dacitic AEMs (Fig. 6a–d). As for amphibole compositions, silica distribution diagrams also record the transition from bimodal melt compositions at the beginning of the Spirit Lake stage to a more continuous spectrum of compositions in younger tephtras that correlate with the appearance of medium-Al MgHst/Tsch.

Trace element compositions of AEMs calculated from high-Al MgHst/Tsch and low-Al MgHbl are relatively low, with constant or slightly increasing values from andesitic to rhyolitic equilibrium melts ($\text{Nb} = 2\text{--}9$ ppm, $\text{La} = 4\text{--}14$ ppm, $\text{Zr} = 40\text{--}114$ ppm, Fig. 6). In contrast, AEMs from medium-Al MgHst/Tsch show a

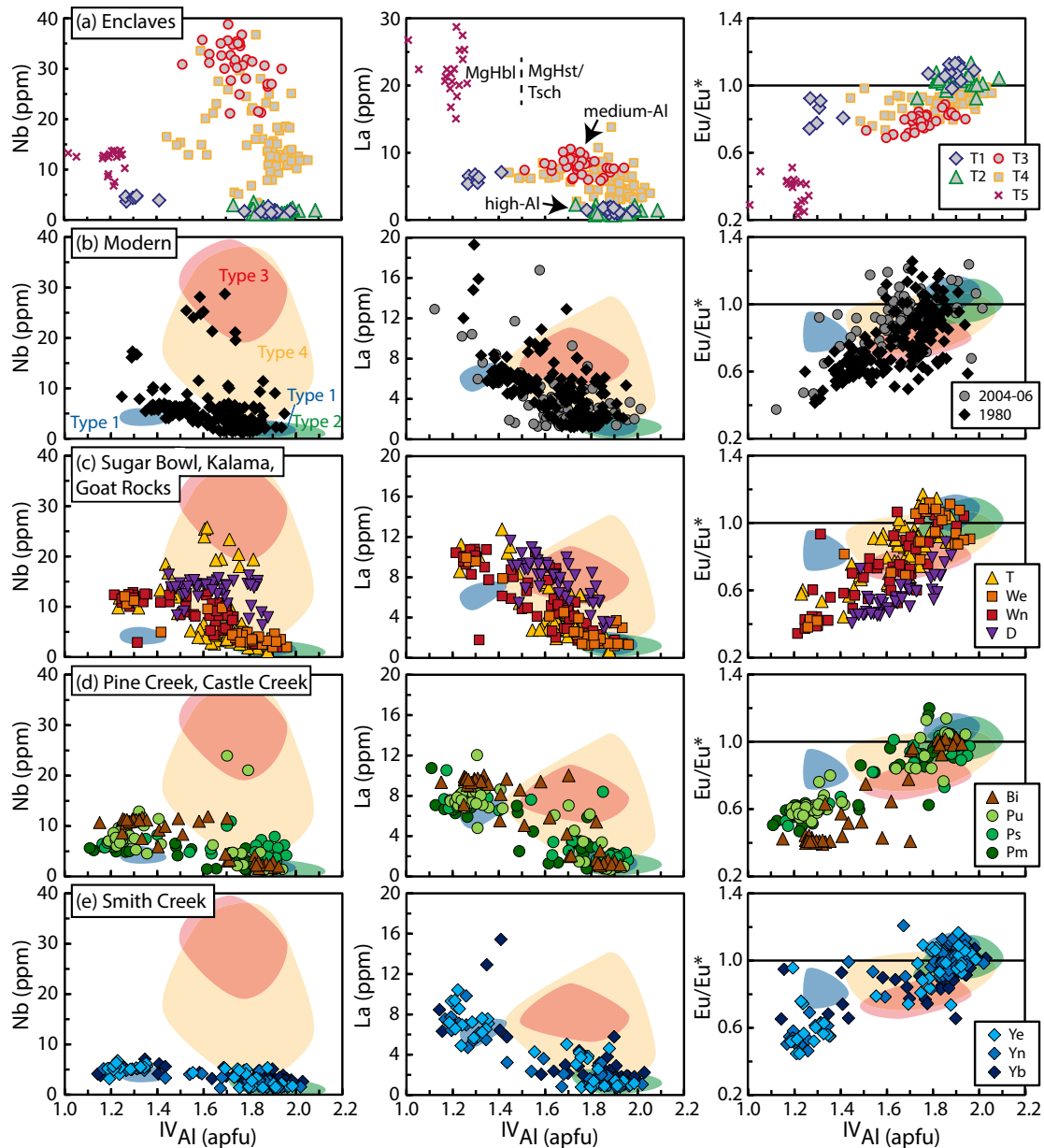


Fig. 4. Trace element composition of amphiboles in mafic enclaves (a) and dacitic tephtras (b–e) from MSH. Units are shown in distinct colors. Eruptive periods are displayed in stratigraphic order from bottom to top with variable symbol shapes; uppermost panels show co-magmatic and xenolithic gabbronorite enclaves. Colored fields in (b) to (e) indicate compositions of amphiboles from mafic enclaves. Amphibole data for the 1980 and 2004–2006 eruptions in (b) are taken from Humphreys *et al.* (2019) and Thorber *et al.* (2008), respectively. MgHbl, magnesiohornblende; MgHst, magnesiohastingsite; Tsch, tschermakite. Average 1σ uncertainties are smaller than the plotted symbol size.

wider compositional range regarding trace element contents extending to higher Nb, La, and Zr concentrations (Fig. 6a–d). All calculated melts of amphiboles from the various dacitic tephtras and mafic enclaves show slightly increasing La/Yb and relatively constant Dy/Yb ratios with increasing SiO_2 (Fig. 7). Some grains in Smith Creek tephtras (set Y), in contrast to younger dacites, show a spread in AEMs toward higher La/Yb and Dy/Yb ratios at rhyolitic melt compositions (Fig. 7e). The Eu anomaly (Eu/Eu^*) in AEMs continuously decreases from 0.9–1.4 (mostly around 1) to 0.4–0.6 with increasing SiO_2 (Fig. 7). At the same time, Sr decreases from ~450 to 600 ppm (up to 630 ppm in type 4 AEM) in basaltic andesitic/andesitic melts toward 75–200 ppm at evolved rhyolitic melt compositions (Suppl. Fig. 8).

Pre-eruptive parameters Temperature and oxygen fugacity

Variations in amphibole populations and composition are accompanied by significant changes in pre-eruptive conditions throughout the Spirit Lake stage. Smith & Leeman (1987) and Gardner *et al.* (1995a) reported two heating trends from the Smith Creek to Castle Creek time and from the Kalama time to 1980 based on Fe–Ti oxide thermometry. We additionally calculated pre-eruptive temperatures and oxygen fugacities ($f\text{O}_2$) in our samples from 258 co-existing magnetite–ilmenite pairs (Sauerzapf *et al.*, 2008, Fig. 8). Each oxide pair was in contact with each other and with melt and fulfilled the Mg/Mn equilibrium criteria of Bacon & Hirschmann (1988). The calculated temperatures increase first from 760 °C in the Yb tephra (Smith Creek period) to 870 °C in the Bi tephra

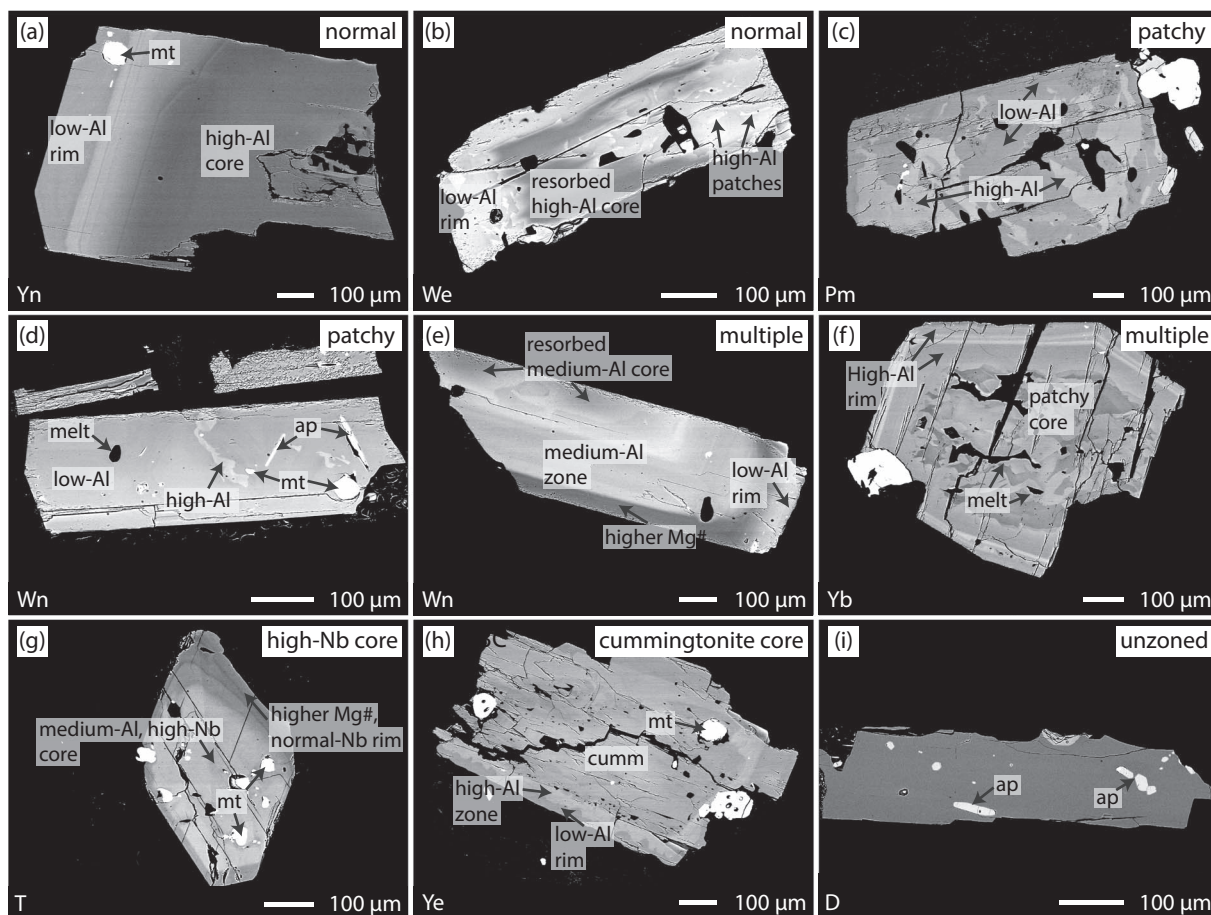


Fig. 5. Backscattered electron images showing a selection of different zoning types in amphibole tephra from MSH: (a, b) normal zoning with variable resorbed high-Al cores and low-Al rims, (c, d) patchy zoning with light, high-Al and dark, low-Al patches, (e) multiple zoning with a resorbed medium-Al core and an inner dark, high-Mg# zone and a low-Al rim, (f) multiple/reverse zoning with a patchy core and an internally zoned high-Al rim, (g, h) xenocrystic cores composed of (g) enriched, medium-Al, high-Nb calcic amphibole and (h) cummingtonite, overgrown by 'normal' calcic amphibole, (i) unzoned, medium-Al amphibole. mt, magnetite; ap, apatite; cumm, cummingtonite.

in the Castle Creek period (average values; error ± 50 °C, Fig. 8), while oxygen fugacities decrease simultaneously from NNO + 2 to NNO + 0.8 (error ± 0.4 log units; Fig. 8; Suppl. Table 5). Subsequently, pre-eruptive temperatures drop to 810 °C in the Wn tephra (Kalama period) and increase again to 890 °C in the T tephra (Goat Rocks period). In contrast to temperatures, oxygen fugacity remains constant here at NNO + 0.8 to +1 (Fig. 8). Conditions for the T tephra are close to those of the Plinian phase of the eruption on May 18, 1980 (870–875 °C and NNO + 0.8; Blundy *et al.*, 2008).

Water content

Temperature changes correlate well with variations in pre-eruptive water contents (Fig. 8). We calculated the water contents of the dacitic magmas from average plagioclase rim and glass compositions (Waters & Lange, 2015). The averaged rim and glass compositions meet the required equilibrium criterion defined in Putirka (2008) for all units except unit Pm of the Pine creek period, which contains significantly more silicic glass. We applied maximum and minimum temperature estimates from Fe-Ti oxide thermometry and an upper crustal pressure of 200 MPa (error ± 0.35 wt% H₂O; an increase of 100 MPa leads to a decrease in water content of ~ 0.1 wt%). The strong temperature dependence of the hygrometer produces a range of water concentrations for each unit, yet variable water concentrations

among the individual units are well resolved (Fig. 8): Water contents significantly decrease from the oldest Yb and Yn tephra in the Smith Creek period (6.9–7.6 wt% H₂O) to the Bi tephra 4.4–4.9 wt% in the Castle Creek period (Fig. 8; Suppl. Table 7) simultaneous to the first heating trend. The following Wn tephra (Kalama period) yields elevated H₂O concentrations (5.4–6.3 wt%) that decline again to the younger T tephra (Goat Rocks period; 3.7–5.2 wt%) coinciding with the second heating trend. Overall, our estimated water contents appear in good agreement with experimental determinations and plagioclase hygrometry (Gardner *et al.*, 1995c; Fig. 8). Melt inclusions from 1980 to 1986 eruptions contain water contents up to 6.7 wt%, again yielding elevated water concentrations (Blundy *et al.*, 2008).

DISCUSSION

Amphiboles in dacitic MSH tephra show a wide range of textures and compositions that indicate changes in magmatic conditions during magma evolution at depth and over time (Figs 3, 4b–e, and 5; Table 1). A progression from bimodal amphibole compositions separated in a high-Al MgHst/Tsch and a low-Al MgHbl population in the Smith Creek period toward a more continuous distribution of amphibole compositions spanning the whole compositional range but centered at medium Al₂O₃ contents, paired with increasing concentrations of incompatible

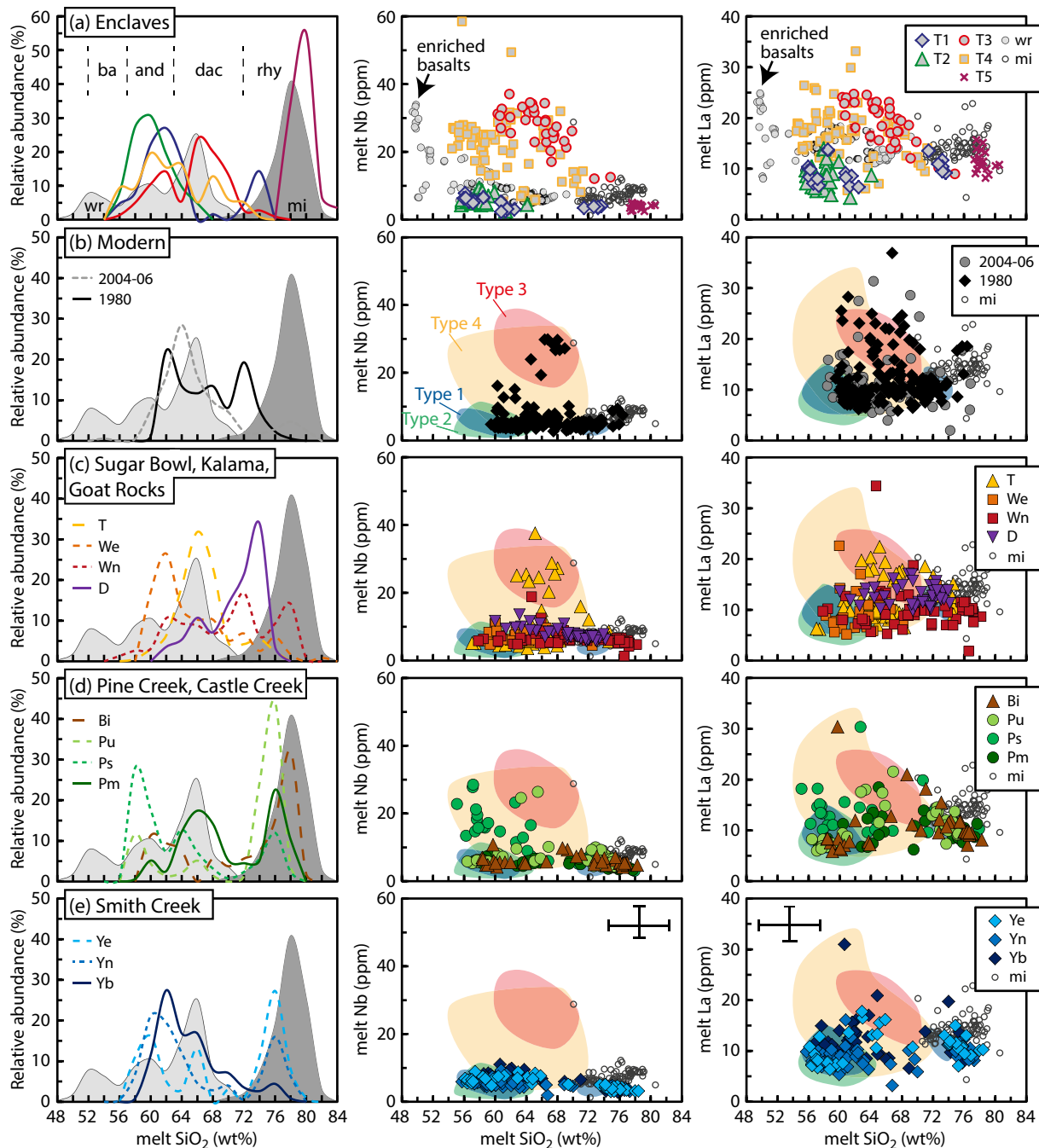


Fig. 6. Compositions of AEMs in mafic enclaves (a) and dacitic tephtras (b–e) from MSH calculated after Zhang *et al.* (2017) and Humphreys *et al.* (2019). Eruptive periods are displayed in stratigraphic order from bottom to top with distinct symbol shapes; uppermost panels show mafic enclaves. Symbols and sources for 1980–2008 dacites as in Fig. 4. Left panels show histograms of SiO₂, middle and right panels Nb and La vs. SiO₂. Compositions of melt inclusions (mi) are taken from Blundy *et al.* (2008), and whole rock (wr) compositions from Wanke *et al.* (2019b). Histograms include unpublished whole rock data from M. Clynne. Note that higher amounts of different mafic units bias the whole rock analyses toward basaltic and andesitic compositions. Dashed lines indicate compositional ranges of basaltic andesite (ba), andesite (and), dacite (dac), and rhyolite (rhy). Representative error bars indicate $\pm 1\sigma$ confidence intervals for each element based on the regression statistics from Humphreys *et al.* (2019).

elements during the last 1000 years, indicates that magma compositions became more diverse throughout the Spirit Lake stage (3900 years BP - present, Fig. 3). Amphiboles from magmatic enclaves record similar distinct populations, which can help to interpret the diversity of amphiboles found in the dacitic tephtras.

Origin of co-magmatic enclave amphiboles

Amphiboles in type 1 and 2 enclaves are predominantly classified as high-Al MgHst/Tsch with few low-Al MgHbl rims

found in type 1 enclaves (Figs 3c and 4a), which are similar to high- and low-Al amphiboles found in MSH dacites. The presence of decomposed rims around high-Al cores from type 2 enclaves (Fig. 2b), however, suggests that low-Al rims may also have been present in type 2 enclaves, forming similar compositional gaps as amphiboles from type 1 enclaves. A pronounced Al-Tschermaks substitution (mostly ^{VI}Al=0.3–0.5 apfu) in MgHst/Tsch cores compared to MgHbl rims (^{VI}Al=1.5–2.5 apfu; Fig. 9a) suggests crystallization of MgHst/Tsch in a deeper

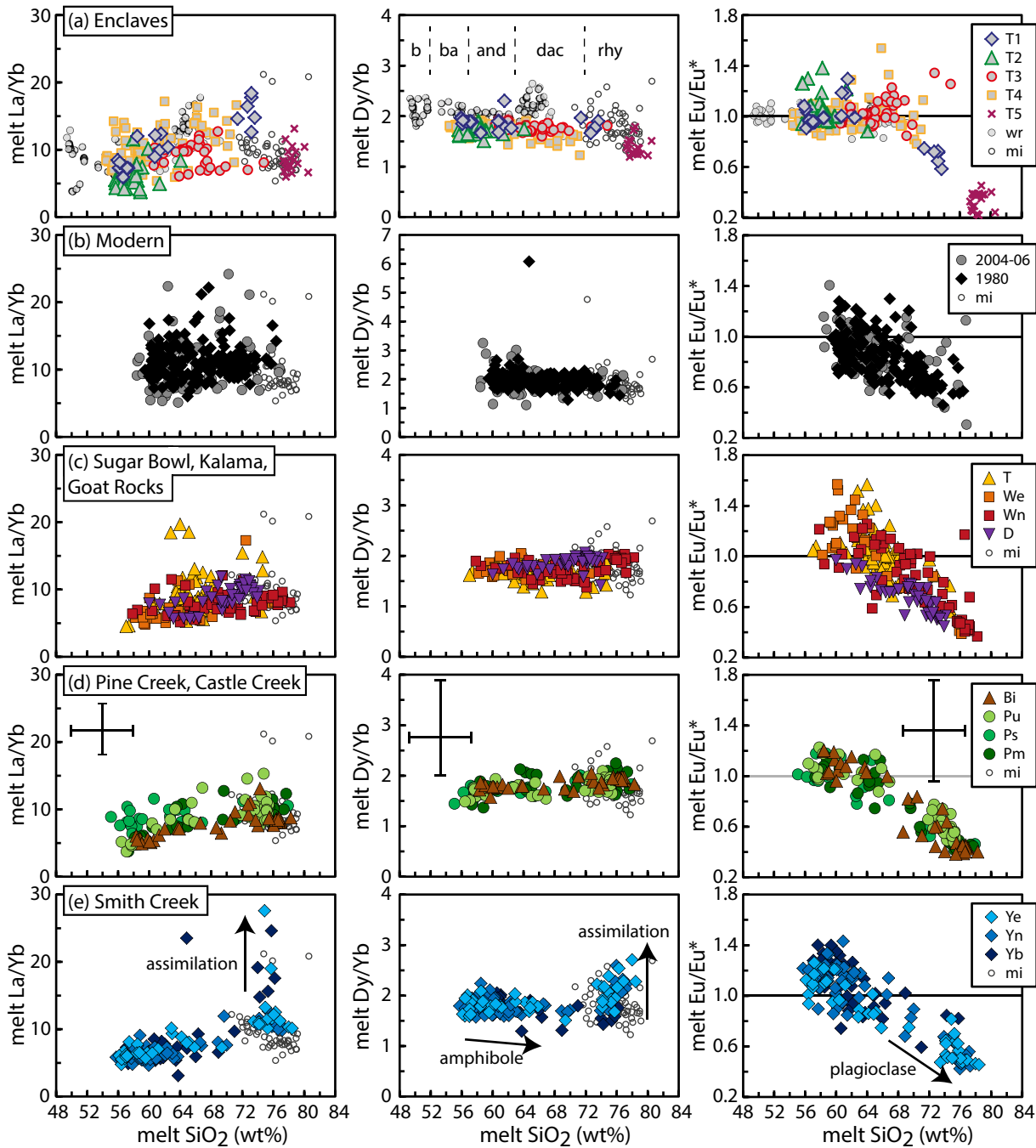


Fig. 7. Compositions of AEMs in mafic enclaves (a) and dacitic tephras (b–e) from MSH calculated after Zhang et al. (2017) and Humphreys et al. (2019). Eruptive periods are displayed in stratigraphic order from bottom to top with distinct symbols; uppermost panels show mafic enclaves. From right to left: La/Yb, Dy/Yb, and Eu/Eu* vs. SiO₂. Eu/Eu* = Eu_N/√(Sm_N*Gd_N), subscript N indicates normalization to chondrite values (Sun & McDonough, 1989). Dashed lines indicate compositional ranges of basalt (b), basaltic andesite (ba), andesite (and), dacite (dac), and rhyolite (rhy). Arrows illustrate amphibole-dominated fractionation at andesitic melt composition, plagioclase-dominated crystallization at rhyolitic melt composition, and assimilation of crustal material at rhyolitic melt compositions in Smith Creek tephras. Calculation uncertainties are given as 1σ error bars.

and more mafic environment than the rims. High-Al MgHst/Tsch in type 1 and 2 enclaves are chemically similar to those in the tephras, although more restricted to mafic compositions and low abundances of incompatible trace elements (Figs 3 and 4). In contrast, MgHbl show higher Mg#, a less pronounced negative Eu anomaly, and generally lower abundances of REE elements compared to most amphiboles from MSH tephras (Fig. 4a, Suppl. Fig. 4) indicating crystallization under slightly less evolved conditions.

The most mafic AEM are compositionally similar to the arc-type basaltic andesite erupted during the Castle Creek period, suggesting a genetic relationship to such magma, as proposed for similar high-Al MgHst/Tsch from Yn and Ye dacites (Wanke et al., 2019b). AEMs with SiO₂ contents of 55–66 wt% and low contents of incompatible trace elements (Fig. 6a) reflect melt evolution from mafic to intermediate compositions, whereas low-Al MgHbl rims crystallized from more siliceous melt (SiO₂ = 71–74 wt%). Accordingly, these enclaves can be interpreted as remnants of

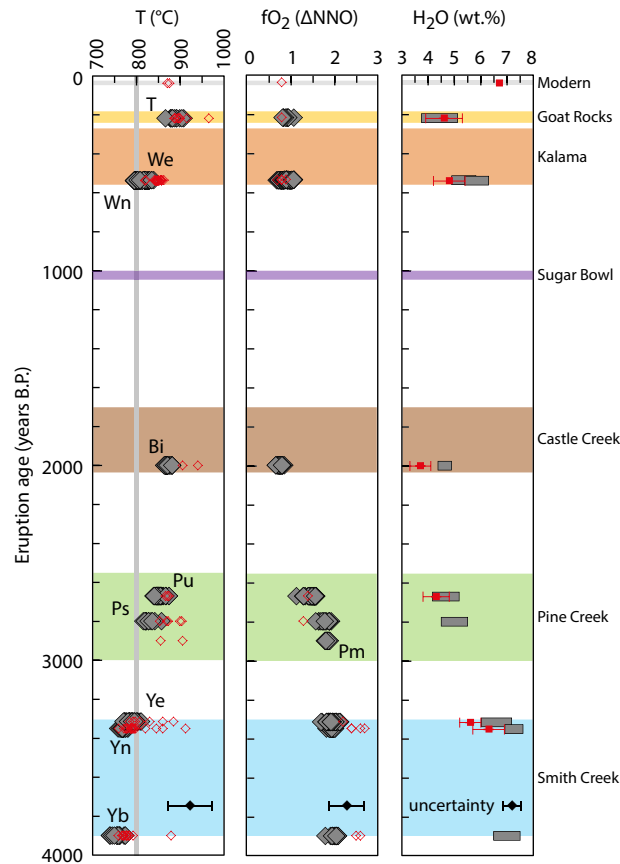


Fig. 8. Changes in pre-eruptive magmatic conditions in major dacitic tephra layers of MSH throughout the Spirit Lake stage. Temperature and oxygen fugacity (fO_2) are calculated from touching magnetite–ilmenite pairs using the method of Sauerzapf *et al.* (2008). Water contents are estimated by plagioclase hygrometry (Waters & Lange (2015)). Water contents of unit *Pm* acquired in this study do not fulfill the equilibrium criterion of Putirka (2008) for plagioclase–liquid pairs and are therefore excluded from this plot. Red empty symbols show data from Smith & Leeman (1987), Gardner *et al.* (1995a), Gardner *et al.* (1995b), and Blundy *et al.* (2008). The gray line indicates the upper thermal stability limit of cummingtonite (Geschwind & Rutherford, 1992).

an intermediate, calc-alkaline recharge magma that crystallized before mixing with the upper crustal mush reservoir (potentially in a cooler marginal zone).

Amphiboles found in type 3 and 4 co-magmatic enclaves exhibit a wider spectrum of AEM covering the compositional gap of amphiboles from type 1 (and 2) enclaves (Fig. 6a). At basaltic andesitic composition, the TiO_2 (1.2–1.9 wt%) and K_2O (1.7–2.8 wt%) contents in type 3 and 4 AEM significantly exceed that of type 1 and 2 AEMs ($TiO_2 = 0.7–1.1$ wt%, $K_2O = 0.4–1.3$ wt%; Suppl. Table 4), forming distinct trends toward more evolved compositions.

They further show significant enrichment in incompatible elements (as found in some amphibole grains in MSH dacites, Figs 6a and 7), indicating that parental melts from type 3 and 4 enclaves are chemically distinct from the arc-type basaltic andesites suggested for type 1 and 2 enclaves. The high abundance of Ti, K and incompatible trace elements in type 3 and 4 melts (Fig. 6a), however, implies a relation of these melts to the previously described HFSE-rich basalts (Wanke *et al.*, 2019b), as do the similar whole rock compositions (enriched incompatible trace element patterns of enclaves resemble those of more mafic HFSE-rich basalts; Suppl. Fig. 3). Such an interpretation is supported by the crystallization of amphibole at the expense of olivine in the basaltic andesite enclaves (type 4; Fig. 2d).

The different trends in key substitution mechanisms between amphiboles from type 3 and 4 enclaves and those from type

1 and 2 enclaves (Fig. 9a, Suppl. Fig. 9a) clearly reflect their different origins. The pressure-sensitive Al-Tschermak substitution is hardly visible in type 3 and 4 MgHst/Tsch (^{IV}Al is constantly around 0.1–0.3 apfu), similar to MgHbl (Fig. 9a), whereas the temperature-sensitive Ti-Tschermak substitution shows a distinct trend ($Ti = 0.55–0.2$ apfu) with decreasing ^{IV}Al , which is significantly higher than that of type 1 and 2 amphiboles, accompanied by a decrease of the temperature-sensitive edenite substitution ($\Delta(Na + K) = 0.65–0.3$, Fig. 9b, Suppl. Fig. 9). These observations are consistent with an origin of type 3 and 4 enclaves by shallow crystallization during isobaric cooling of hot, Ti-rich magma, as expected from intrusion of HFSE-rich basalts/basaltic andesites into the shallow dacitic mush zone. The scarce presence of co-magmatic enclaves at MSH suggests that the mixing efficiency between recharge magmas and sub-volcanic mush is generally high, making it difficult to determine the relative amounts of recharge magmas below MSH.

Origin of the different amphibole populations The high- and low-Al amphibole populations

The pronounced compositional gap between high-Al MgHst/Tsch and low-Al MgHbl (Fig. 3c and d) and the often-resorbed nature of high-Al MgHst/Tsch cores overgrown and partly replaced by euhedral low-Al MgHbl rims (Fig. 5a–d) indicate that the two amphibole populations crystallized from different magmas stored at distinct magmatic conditions. Relics of high-Al cores usually record higher

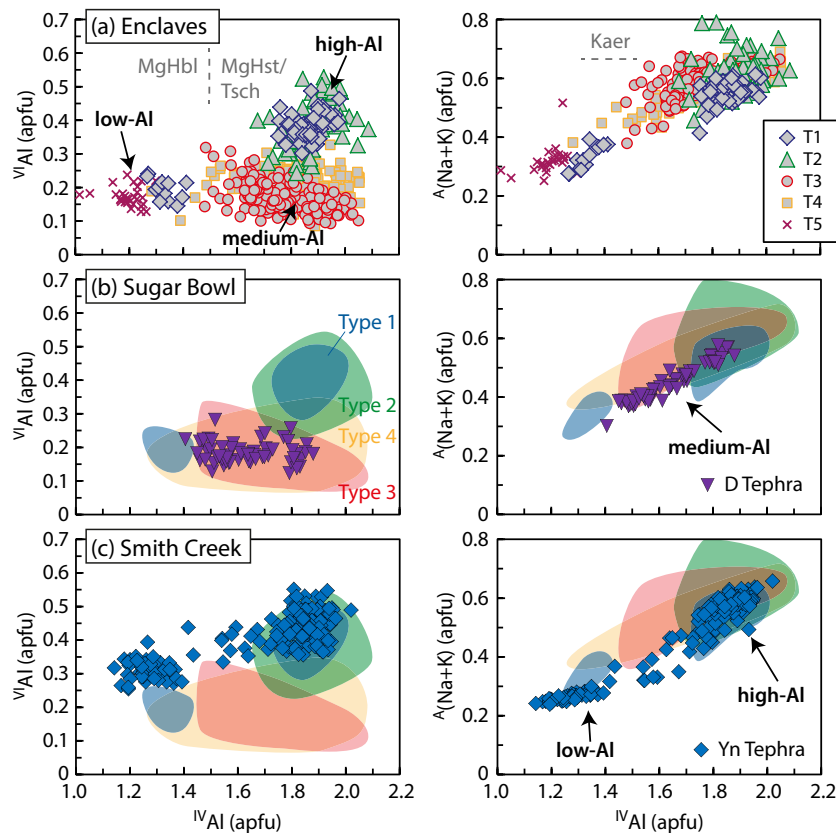


Fig. 9. Variations in the pressure-sensitive Al-Tschermaks (left) and temperature-sensitive Edenite (right) exchange in amphiboles from mafic enclaves (a) and selected dacitic tephtras (b, c) of MSH. The Ye tephra occurring at the end of the Smith Creek period (c) contains high-Al MgHst/Tsch and low-Al MgHbl, while the D tephra erupted during the Sugar Bowl period (b) contains exclusively medium-Al MgHst/Tsch. Averaged 1σ uncertainties are smaller than the plotted symbol size.

contributions of the Al-Tschermak, Ti-Tschermak, and edenite substitutions [i.e. higher VAl , Ti, and $A(Na+K)$] compared to low-Al MgHbl, which suggests their crystallization at higher temperatures and pressures than low-Al MgHbl rims (Fig. 9c; Suppl. Fig. 9). AEMs of high-Al MgHst/Tsch cores furthermore yield basaltic andesite to low- SiO_2 dacite compositions (Fig. 6b–e) with a lack of or only weak negative Eu-anomalies (Figs 4b–e and 7), indicating the suppression of plagioclase crystallization during the growth of such amphiboles. Slightly increasing La/Yb ratios at nearly constant Dy/Yb ratios, therefore, suggest amphibole-dominated fractionation of the melts producing high-Al amphiboles in deep, hydrous conditions. Based on these observations, high-Al MgHst/Tsch cores are interpreted to represent crystal cargo from a lower crustal storage zone, as supported by the experimental determination of MSH Yn dacite formation pressures (700–900 MPa, Blatter et al., 2017) and seismic and magnetotelluric evidence for a mid- to lower crustal magma reservoir (Hill et al., 2009; Kiser et al., 2016; Bedrosian et al., 2018). In contrast to the partially resorbed high-Al cores, compositionally similar but idiomorphic high-Al MgHst/Tsch outer zones in complexly zoned crystals (e.g. around low-Al MgHbl or cummingtonite; Fig. 5f and h; the latter restricted to 200–300 MPa; Geschwind & Rutherford, 1992), must have crystallized at shallow depths and were probably formed after recharge of and mixing with more mafic magma, consistent with more mafic AEM.

Low-Al MgHbl zones contain lower VAl , Ti, and $A(Na+K)$ that indicate their crystallization at lower temperatures and pressures than the high-Al amphibole cores (e.g. Putirka, 2016, Fig. 9c, Suppl. Fig. 9). However, similar melt compositional signatures

suggest a genetic relation between the two crystal types (Figs 6 and 7). This effect can be caused by the ascent of silicic andesitic to dacitic magma from the lower crust, where high-Al cores were formed, into a cooler and more evolved mid to upper crustal magma reservoir beneath MSH (as outlined for the 1980–1986 eruptions; Pallister et al., 2017; Pallister et al., 2008; Scandone & Malone, 1985). Magma ascent to and crystallization at shallow depth are also supported by the co-crystallization of plagioclase, evident from lower Sr contents and pronounced negative Eu-anomalies in rhyolitic AEM calculated from low-Al MgHbl rims (Figs 4b–e and 7). The lack of Eu-anomalies in whole rocks from MSH (Suppl. Fig. 3) additionally indicates that crystal-melt separation in the upper crust is not very efficient, forming high-crystallinity magmas (25–50 vol %; Gardner et al., 1995b) containing plagioclase \pm MgHbl \pm oxide \pm pyroxene \pm apatite.

Frequent rejuvenation of the upper crustal mush by intruding magmas of various compositions generates the textural and compositional complexity of MSH dacites (Blundy et al., 2008; Cashman & Blundy, 2013), which is also evident in the amphibole textures (Fig. 5).

The trace element-enriched, medium-Al MgHst/Tsch

The most striking feature of variably trace element-enriched, medium-Al MgHst/Tsch is their sudden appearance during Pine Creek time and continued presence thereafter (Table 1). They show nearly constant VAl with decreasing $IVAl$, while Ti and $A(Na+K)$ decrease (Fig. 9b, Suppl. Fig. 9a–d), indicative of crystallization during isobaric cooling conditions. Even at high $IVAl$, medium-Al MgHst/Tsch exhibit similar Al^{VI} concentrations

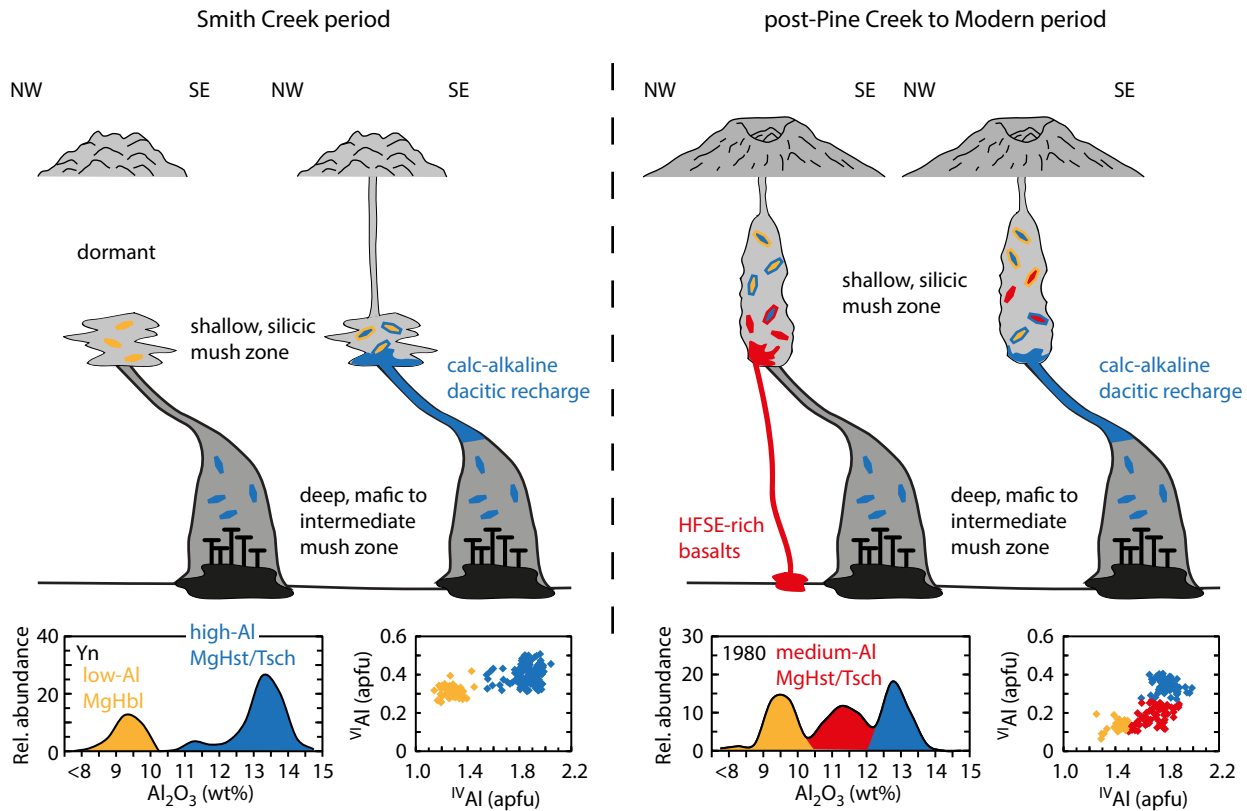


Fig. 10. Schematic cartoon of the magmatic plumbing system beneath MSH during the Smith Creek and post-Pine Creek eruptive periods. Al_2O_3 content in amphiboles is exemplarily shown for Yn and 1980 dacites. Amphibole compositions for 1980 eruptions are taken from Humphreys *et al.* (2019). The offset geometry of the system is suggested by seismic data (Kiser *et al.*, 2016). In post-Pine Creek time, the upper crustal reservoir is vertically extended toward shallower depth, and incompatible trace element enriched mafic magma causes crystallization of enriched medium-Al $_2\text{O}_3$ MgHst/Tsch. MgHbl, magnesiohornblende; MgHst, magnesiohastingsite; Tsch, tschermakite.

as low-Al MgHbl, pointing to shallow crystallization depths of the medium-Al amphiboles in the upper crust. The (variable) enrichment of medium-Al MgHst/Tsch in incompatible elements (Fig. 4b–d) is also reflected by their intermediate (54–70 wt% SiO_2) AEM (Fig. 6b–d), filling the observed compositional gap between low- and high-Al amphiboles. Humphreys *et al.* (2019) interpreted such enriched, intermediate AEM of 1980 amphiboles as the result of remelting and assimilation of cumulates and/or mixing with trace element-enriched, mafic magma, such as HFSE-rich basalts erupted during the Castle Creek period (Smith & Leeman, 1993; Leeman & Smith, 2018; Wanke *et al.*, 2019a). Remelting and assimilation of an amphibole-oxide-apatite-zircon-biotite-bearing crystal mush could potentially lead to the observed enrichment in Ti, K, REE, Nb, and Zr. However, the abundance of enriched, medium-Al MgHst/Tsch in distinct co-magmatic enclaves (types 3 and 4, with a suggested relation to HFSE-rich basalts) that also show trace element-enriched whole rock compositions (Fig. 1, Suppl. Fig. 3), indicate that these amphiboles derive from HFSE-rich basalts or basaltic andesites (such as type 4 basaltic andesite enclaves) entering the upper crustal magma reservoir (Fig. 10). Coombs & Gardner (2004) have shown that magnesian olivine forms amphibole reaction rims when in contact with a silicic melt. Accordingly, crystallization of medium-Al MgHst/Tsch at the expense of olivine, as observed in type 4 enclaves (Fig. 2d), supports an origin during mixing with evolved upper crustal mush. This process is well reflected by the disaggregation of type 4 enclaves (Suppl. Fig. 1d). Likewise the increasing complexity of the observed zoning patterns supports the theory that magma mixing played an important role.

As a consequence, the appearance of medium-Al MgHst/Tsch concurrently with increasing pre-eruptive temperature and decreasing water content and oxygen fugacity in the dacites during Pine Creek time (Fig. 8) marks the appearance of HFSE-rich basalts in the upper crustal system.

Tracing the evolution of the plumbing system over time

The structure of the sub-volcanic plumbing system

In contrast to many other arc volcanoes with typical bimodal amphibole populations [e.g. Mt. Hood (Kent, 2014), Soufrière Hills volcano (Rutherford & Devine, 2003), Redoubt Volcano (Coombs *et al.*, 2013), Mt. Pelée (Pichavant *et al.*, 2002), Shiveluch volcano (Humphreys *et al.*, 2006), Ciomadul volcano (Kiss *et al.*, 2014)], MSH dacite tephra (especially the younger units) record more continuous amphibole compositional spectra through the abundant presence of medium-Al amphiboles (Fig. 3a and b). This divergence at MSH has previously been attributed to amphibole crystallization over a continuous pressure range by melt ascent in a large, vertically extended magma reservoir reaching from the mid to the upper crust beneath MSH (Rutherford & Devine, 2008; Thornber *et al.*, 2008; Ridolfi *et al.*, 2010; Turner *et al.*, 2013). However, a continuous trans-crustal magma reservoir beneath MSH may be questioned if we consider that (1) the amphibole population in pre-Sugar Bowl dacites is indeed predominantly bimodal with low-Al MgHbl and high-Al MgHst/Tsch (Fig. 3c and d) and that (2) both low-Al MgHbl and high-Al MgHst/Tsch remain present throughout the whole Spirit Lake stage (Fig. 4; Suppl. Fig. 9).

We, therefore, propose that medium-Al amphiboles at MSH formed during the mixing of HFSE-rich basalt with dacitic melts in an upper crustal reservoir. This upper crustal reservoir typically produces low-Al MgHbl (and sometimes crystal zones of high-Al MgHst/Tsch in response to mafic recharge events), while relics of high-Al amphibole cores crystallized from calc-alkaline basaltic andesitic to dacitic melts in the lower crust (Fig. 10). Thus, we suggest that the wide range of amphibole compositions at MSH reflects the diversity of mafic magmas in the system rather than large pressure variations. Underlining this interpretation, previous studies show that the amphibole chemistry is primarily controlled by the parent-melt chemistry and, to a lesser extent, by its pressure (Erdmann et al., 2014; Kiss et al., 2014; Zhang et al., 2017). Consequently, the major difference between MSH and many other andesitic to dacitic arc volcanoes is not necessarily the outline and position of the upper crustal magma reservoir(s), but rather the diversity of mafic magma types that cross the upper crustal magmatic system and erupt in close spatial and temporal proximity to andesites and dacites.

Relative changes in the pressure-sensitive Al-Tschermaks substitution in late-crystallizing MgHbl rims, however, may suggest an extension of the upper crustal magma reservoir to shallower depth throughout the Spirit Lake stage. MgHbl rims show a drop in ^{VI}Al from 0.25–0.35 apfu in Smith Creek dacites to 0.15–0.25 apfu in Castle Creek dacites, and a larger range in most younger dacites (0.1–0.3 apfu; Suppl. Fig. 9b–e), supporting depth changes and a vertical extension of the upper crustal magma storage region as proposed by Gardner et al. (1995c). Crystallization pressures for amphiboles in Smith Creek tephra are well established by the presence of cummingtonite (200–300 MPa; Geschwind & Rutherford, 1992), corresponding to ~9–12.5-km depth, in the Smith Creek dacites (3900–3300 years BP). In contrast, magma feeding the eruption on May 18, 1980 was supplied from the top of a reservoir that extended from ~6- to 13-km depth (Scandone & Malone, 1985). The observed vertical extension of the magmatic system to shallower levels throughout the Spirit Lake stage (Fig. 10) was likely induced by heating and fracturing of the overlying wall rocks during the maturation of the system (Townsend et al., 2019). This is consistent with the predominant occurrence of xenolithic gabbroic enclaves (type 5, presumably wall rocks) in eruptions following large Plinian eruptions.

Tracing a magmatic component through time and space

Smith Creek eruptive period (3900–3300 years BP)

Dacitic tephra from the Smith Creek period yield a bimodal distribution of amphibole composition (Fig. 3d), typical for intermediate arc volcanoes (Kent, 2014). In combination with amphibole textures and calculated AEM, this suggests crystallization of high-Al MgHst/Tsch from calc-alkaline, mafic magma evolving in the lower crust and recharge of the resulting dacitic magma into an upper-crustal silicic reservoir, where low-Al MgHbl crystallizes from rhyolitic melt. Frequent rejuvenation of this mid to upper crustal mush by more mafic, calc-alkaline magma forms multiple-zoned amphibole crystals.

Pine Creek to Castle Creek eruptive periods (3000–1700 years BP)

The ubiquitous presence of medium-Al MgHst/Tsch in post-Pine Creek dacites reflects some contribution of HFSE-rich basalts to MSH dacites since ~2900 years (Figs 3c and 4d; Table 1). In addition, crystallization temperatures increase from 760 to 800 °C in Smith Creek dacite to 800–850 °C in early Pine Creek dacite

and to 860–880 °C in Castle Creek dacite (Fig. 8), concomitant with higher contributions of the temperature-sensitive Ti-Tschermaks and edenite substitutions in the amphibole structure [higher Ti and $^A(Na + K)$; Suppl. Fig. 9d] of low-Al MgHbl. The concurrent appearance of medium-Al MgHst/Tsch and increasing abundance along with a change of pre-eruptive conditions in the dacites toward higher temperature and lower water content and oxygen fugacity (Fig. 8) is consistent with an increase of this mafic component in the upper crustal system from Pine Creek to late Castle Creek time, when HFSE-rich basalts erupted (2025–1700 years BP, Wanke et al., 2019a). This process is reflected in the increasingly frequent, mafic, and less explosive eruptions over the course of the Smith Creek-Pine-Creek-Castle Creek cycle (Hopson & Melson, 1990) and the appearance of mafic enclaves in Pine Creek dacite.

Sugar Bowl rhyodacite (1050–1000 years BP)

In contrast to other dacitic tephra, amphiboles in the following Sugar Bowl rhyodacite are restricted to the medium-Al MgHst/Tsch population (Fig. 3b). Constantly low ^{VI}Al (Fig. 9b), abundant inclusions of Fe-Ti oxides and apatite (Fig. 5i), and intergrowth with orthopyroxene point to shallow crystallization depths. In addition, this is the only unit that comprises abundant unzoned amphiboles as well as diffusive zoning patterns. Such crystals likely derive from diffusive re-equilibration during prolonged storage. Combined with equilibrium melt compositions of 60 to 75 wt% SiO₂, these observations suggest that the Sugar Bowl rhyodacite may have evolved from remnants of Castle Creek magma during ~1000 years of storage in the uppermost crust without significant further mafic recharge. That is consistent with the experiments of Riker et al. (2015), which indicate that much of the textural and compositional complexity in plagioclase and pyroxene in Sugar Bowl rhyodacite does not require mixing, cooling, or decompression. Instead, textural complexity can be explained by variations in the bulk volatile content of the crystallizing magma and by crystallization of minerals along different degassing pathways, which can alter the dissolved volatile content around crystallizing mineral grains and induce a heterogeneous distribution of volatiles in the magma reservoir.

Kalama to recent eruptive periods (1479 CE–today)

The following Kalama cycle started with the voluminous eruption of tephra layer Wn. Abundant MgHbl crystals with only small relics of high-Al patches (Fig. 5d) and mostly low contributions of the Al-Tschermak substitution (low ^{VI}Al , Suppl. Fig. 9b and c) likely reflect crystallization of MgHbl during storage and melt evolution in the uppermost part of the system, potentially filling the previous Sugar Bowl reservoir. Yet, the textural diversity in Wn amphibole and the abundance of medium-Al MgHst/Tsch compositions reflect a largely extending upper crustal reservoir that was variably influenced by different types of mafic magma. The following We dacite has similar amphibole textures and compositions but contains almost no shallow-crystallizing MgHbl, consistent with magma ascent from greater depth, within only 2 years after the Wn eruption (Table 1). Besides abundant medium-Al MgHst/Tsch compositions, quenched mafic enclaves (type 4) in early Kalama dacite domes represent a minor HFSE-rich basalt component. Increasing pre-eruptive temperatures and decreasing water contents from the early Kalama to the Goat Rocks and modern dacites (Fig. 8) reflect an increasing basalt component in MSH dacites. Extensive eruptions of mixed andesites in the mid Kalama time (Pallister et al., 1992; Smith & Leeman, 1993) indicate almost equal amounts of enriched basalt and eruptible dacite in the upper part of the system. Afterward, the basalt component

ceased again, and SiO₂ contents in subsequent Kalama eruptions remained ≥ 61 wt%. Yet, the common presence of medium-Al MgHst/Tsch in Goat Rocks, 1980, and 2004–2006 dacite (Fig. 3b) still records minor amounts of basaltic magma entering the upper crustal part of the plumbing system. The relative contribution of this basaltic component will likely play an important role in the future behavior of the volcano.

Spatial occurrence of HFSE-rich basalts in the magmatic system

In contrast to low-Al MgHbl and medium-Al MgHst/Tsch, high-Al MgHst/Tsch show nearly constant compositions throughout the Spirit Lake stage (Fig. 4b–e, Suppl. Fig. 9b–e, Suppl. Table 4). These crystals, when appearing in a certain textural context (e.g. resorbed cores surrounded by MgHbl with a distinct compositional gap), are interpreted to trace melt evolution from basaltic andesite toward dacite in the lower crust. Their ubiquitous presence in dacitic tephra (except for layer D), thus, indicates that the formation mechanism of MSH dacites in the lower crust (Blatter et al., 2017; Humphreys et al., 2019; Wanke et al., 2019b) remained persistent throughout the last 3900 years. The restricted influence of HFSE-rich basalt on MSH dacites to the mid to upper crustal system indicates that HFSE-rich basalts either largely bypassed the lower crustal magma generation zone and/or that their abundance is negligible compared to normal arc basalt. Isolated pathways through the lower crust are consistent with the eruption of basalt in close spatial and temporal proximity with andesites and dacites (Wanke et al., 2019a) and might be facilitated by an offset structure of the magmatic system suggested by seismic and magnetotelluric anomalies in the crust (Hill et al., 2009; Kiser et al., 2016; Bedrosian et al., 2018).

CONCLUSIONS

Amphiboles can be powerful archives of magmatic processes. This study presents a large textural and chemical database of major and trace element compositions in amphiboles from multiple volcanic units of MSH and clearly demonstrates fluctuating conditions in the magmatic plumbing system in the last 4000 years due to the interaction of different mafic parental magmas with two main reservoirs: one in the upper crust and one in the lower crust. Three different amphibole populations (high-Al MgHst/Tsch, medium-Al MgHst/Tsch, and low-Al MgHbl) have been identified, allowing us to trace magma evolution in the magmatic system over the past 3900 years.

Relics of resorbed high-Al MgHst/Tsch cores trace continuous melt evolution from basaltic andesite to dacite in the lower crust. Low-Al MgHbl crystallizes from rhyolitic melt in shallow reservoirs. The bimodality of the respective melts from which these amphiboles have grown is reflected by calculated AEM compositions. Mafic recharge of the shallow silicic mush zone by HFSE-rich basalts is recorded by trace element-enriched, medium-Al MgHst/Tsch that first appears in Pine Creek tephra from 2900 years BP, marking the change from a previously bimodal to a continuous melt composition. Respective AEM compositions are intermediate and co-magmatic mafic enclaves are rare, both indicating that HFSE-rich basalts mix with the dacitic mush of the shallow reservoir, potentially forming hybrid andesitic melts. The direct contamination of the upper crustal silicic reservoir by HFSE-rich basalts is indicated by increasing crystallization temperatures, drier conditions, and more complex zoning patterns in amphiboles, whereas the deep-crystallizing high-Al MgHst/Tsch remain largely unaffected. This suggests that

the abundance of HFSE-rich basalts is small compared to typical arc basalt and/or that these mainly bypass the lower crustal plumbing system (Fig. 10). The latter hypothesis is consistent with a tilted structure of the plumbing system suggested by seismic and magnetotelluric anomalies in the crust (Hill et al., 2009; Kiser et al., 2016; Bedrosian et al., 2018), with the upper crustal reservoir being shifted westward from the lower crustal reservoir.

Amphiboles allowed us to reveal the complex magmatic plumbing system, reservoir-bypassing recharges, and local hybridization of melts beneath MSH, all happening in just a few thousand years of activity. This very versatile mineral can hence be used as a complementary tool to geophysical imaging/monitoring in volcanically active areas. In particular, we show that a continuous range in major element compositions of amphiboles (from high-Al to low-Al compositions) does not necessarily imply crystallization in a nearly continuous transcrustal mush column but can be produced by mixing, in the upper crust, of diverse magmas stemming from the upper mantle and lower crust.

SUPPLEMENTARY DATA

Supplementary data are available at *Journal of Petrology* online.

FUNDING

This project has been supported by Swiss National Science Foundation grants 200021_146268.

ACKNOWLEDGEMENTS

We thank Michael A. Clynne and John Pallister for a much-appreciated introduction into MSH deposits in the field and for providing access to the sample collection of D. Mullineaux at CVO. We are grateful to Lydia Zehnder, Baptiste Lemirre, Peter Appel, and Barbara Mader for analytical assistance. This manuscript significantly benefited from the helpful and constructive reviews of M. Coombs, P. Shane, and S. Erdmann. A. Kent is thanked for the careful editorial handling of the manuscript.

References

- Alonso-Perez, R., Müntener, O. & Ulmer, P. (2009). Igneous garnet and amphibole fractionation in the roots of island arcs: experimental constraints on andesitic liquids. *Contributions to Mineralogy and Petrology* **157**, 541–558. <https://doi.org/10.1007/s00410-008-0351-8>.
- Anderson, J. L. & Smith, D. R. (1995). The effects of temperature and f_{O_2} on the Al-in-hornblende barometer. *American Mineralogist* **80**, 549–559. <https://doi.org/10.2138/am-1995-5-614>.
- Arculus, R. J. & Wills, K. J. (1980). The petrology of plutonic blocks and inclusions from the Lesser Antilles island arc. *Journal of Petrology* **21**, 743–799. <https://doi.org/10.1093/petrology/21.4.743>.
- Bachmann, O. & Dungan, M. A. (2002). Temperature-induced Al-zoning in hornblendes of the fish canyon magma, Colorado. *American Mineralogist* **87**, 1062–1076. <https://doi.org/10.2138/am-2002-8-903>.
- Bacon, R. C. & Hirschmann, M. M. (1988). Mg/Mn partitioning as a test for equilibrium between co-existing Fe-Ti oxides. *American Mineralogist* **73**, 57–61.
- Bedrosian, P. A., Peacock, J. R., Bowles-Martinez, E., Schultz, A. & Hill, G. J. (2018). Crustal inheritance and a top-down control on arc

- magmatism at Mount St. Helens. *Nature Geoscience* **11**, 865–870. <https://doi.org/10.1038/s41561-018-0217-2>.
- Blatter, D. L., Sisson, T. W. & Hanks, W. B. (2017). Voluminous arc dacites as amphibole reaction-boundary liquids. *Contributions to Mineralogy and Petrology* **172**(5), 1–37. <https://doi.org/10.1007/s00410-017-1340-6>.
- Blundy, J. D., Cashman, K. V. & Berlo, K. (2008) Evolving magma storage conditions beneath Mount St. Helens inferred from chemical variations in melt inclusions from the 1980–1986 and current (2004–2006) eruptions. In: Sherrod D. R., Scott W. E. & Stauffer P. H. (eds) *A volcano rekindled: the renewed eruption of Mount St. Helens, 2004–2006*. USGS Prof Pap 1750, pp.755–790.
- Cashman, K. V. & Blundy, J. D. (2013). Petrological cannibalism: the chemical and textural consequences of incremental magma body growth. *Contributions to Mineralogy and Petrology* **166**, 703–729. <https://doi.org/10.1007/s00410-013-0895-0>.
- Claiborne, L. L., Miller, C. F., Flanagan, D. M., Clynne, M. A. & Wooden, J. L. (2010). Zircon reveals protracted magma storage and recycling beneath Mount St. Helens. *Geology* **38**, 1011–1014. <https://doi.org/10.1130/G31285.1>.
- Clynne, M. A., Calvert, A. T., Wolfe, E. W., Evarts, R. C., Fleck, R. J. & Lanphere, M. A. (2008) The Pleistocene eruptive history of Mount St. Helens, Washington, from 300,000 to 12,800 years before present. In: Sherrod D. R., Scott W. E. & Stauffer P. H. (eds) *A volcano rekindled: The renewed eruption of Mount St. Helens, 2004–2006*. USGS Prof Pap 1750, pp.593–628.
- Coombs, M. L. & Gardner, J. E. (2004). Reaction rim growth on olivine in silicic melts: implications for magma mixing. *American Mineralogist* **89**, 748–758. <https://doi.org/10.2138/am-2004-5-608>.
- Coombs, M. L., Sisson, T. W., Bleick, H. A., Henton, S. M., Nye, C. J., Payne, A. L., Cameron, C. E., Larsen, J. F., Wallace, K. L. & Bull, K. F. (2013). Andesites of the 2009 eruption of redoubt volcano, Alaska. *Journal of Volcanology and Geothermal Research* **259**, 349–372. <https://doi.org/10.1016/j.jvolgeores.2012.01.002>.
- Crandell, D. R. (1987) *Deposits of pre-1980 pyroclastic flows and lahars from Mount St. Helens volcano*. Washington, USGS Prof Pap 1444.
- Davidson, J., Turner, S., Handley, H., Macpherson, C. & Dosseto, A. (2007). Amphibole "sponge" in arc crust? *Geology* **35**, 787–790. <https://doi.org/10.1130/G23637A.1>.
- De Angelis, S. H., Larsen, J. & Coombs, M. (2013). Pre-eruptive magmatic conditions at Augustine volcano, Alaska, 2006: evidence from amphibole geochemistry and textures. *Journal of Petrology* **54**, 1939–1961. <https://doi.org/10.1093/petrology/egt037>.
- Dessimoz, M., Müntener, O. & Ulmer, P. (2012). A case for hornblende dominated fractionation of arc magmas: the Chelan complex (Washington cascades). *Contributions to Mineralogy and Petrology* **163**, 567–589. <https://doi.org/10.1007/s00410-011-0685-5>.
- Erdmann, S., Martel, C., Pichavant, M. & Kushnir, A. (2014). Amphibole as an archivist of magmatic crystallization conditions: problems, potential, and implications for inferring magma storage prior to the paroxysmal 2010 eruption of mount Merapi, Indonesia. *Contributions to Mineralogy and Petrology* **167**, 1016. <https://doi.org/10.1007/s00410-014-1016-4>.
- Gardner, J. E., Carey, S., Rutherford, M. J. & Sigurdsson, H. (1995a). Petrologic diversity in Mount St. Helens dacites during the last 4,000 years: implications for magma mixing. *Contributions to Mineralogy and Petrology* **119**, 224–238. <https://doi.org/10.1007/BF00307283>.
- Gardner, J. E., Carey, S., Sigurdsson, H. & Rutherford, M. J. (1995b). Influence of magma composition on the eruptive activity of Mount St. Helens, Washington. *Geology* **23**, 523–526. [https://doi.org/10.1130/0091-7613\(1995\)023<0523:IOMCOT>2.3.CO;2](https://doi.org/10.1130/0091-7613(1995)023<0523:IOMCOT>2.3.CO;2).
- Gardner, J. E., Rutherford, M., Carey, S. & Sigurdsson, H. (1995c). Experimental constraints on pre-eruptive water contents and changing magma storage prior to explosive eruptions of mount St Helens volcano. *Bulletin of Volcanology* **57**, 1–17. <https://doi.org/10.1007/BF00298703>.
- Geschwind, C.-H. & Rutherford, M. J. (1992). Cummingtonite and the evolution of the Mount St. Helens (Washington) magma system: an experimental study. *Geology* **20**, 1011–1014. [https://doi.org/10.1130/0091-7613\(1992\)020<1011:CATEOT>2.3.CO;2](https://doi.org/10.1130/0091-7613(1992)020<1011:CATEOT>2.3.CO;2).
- Gill, J. B. (1981) *Orogenic andesites and plate tectonics*. Berlin-Heidelberg: Springer-Verlag.
- Guillong, M., von Quadt, A., Sakata, S., Peytcheva, I. & Bachmann, O. (2014). LA-ICP-MS Pb–U dating of young zircons from the Kos-Nisyros volcanic Centre, SE Aegean arc. *Journal of Analytical Atomic Spectrometry* **29**, 963–970. <https://doi.org/10.1039/C4JA00009A>.
- Guillong, M., Meier, D., Allan, M., Heinrich, C. & Yardley, B. (2008). SILLS: a MATLAB-based program for the reduction of laser ablation ICP-MS data of homogeneous materials and inclusions. *Mineralogical Association of Canada Short Course 40*, 328–333.
- Halliday, A. N., Fallick, A. E., Dickin, A. P., Mackenzie, A. B., Stephens, W. E. & Hildreth, W. (1983). The isotopic and chemical evolution of Mount St. Helens. *Earth and Planetary Science Letters* **63**, 241–256. [https://doi.org/10.1016/0012-821X\(83\)90040-7](https://doi.org/10.1016/0012-821X(83)90040-7).
- Hammarstrom, J. M. & Zen, E.-A. (1986). Aluminium in hornblende: an empirical igneous geobarometer. *American Mineralogist* **71**, 1297–1313.
- Heliker, C. (1995). Inclusions in Mount St. Helens dacite erupted from 1980 through 1983. *Journal of Volcanology and Geothermal Research* **66**, 115–135. [https://doi.org/10.1016/0377-0273\(94\)00074-Q](https://doi.org/10.1016/0377-0273(94)00074-Q).
- Higgins, O., Sheldrake, T. & Caricchi, L. (2022). Machine learning thermobarometry and chemometry using amphibole and clinopyroxene: a window into the roots of an arc volcano (mount Liamuiga, saint Kitts). *Contributions to Mineralogy and Petrology* **177**(1), 10. <https://doi.org/10.1007/s00410-021-01874-6>.
- Hildreth, W. S. (2007). Quaternary magmatism in the cascades: geological perspectives. USGS Prof Pap 1744.
- Hill, G. J., Caldwell, T. G., Chertkoff, D. G., Bibby, H. M., Burgess, M. K., Cull, J. P. & Cas, R. A. F. (2009). Distribution of melt beneath mount St Helens and Mount Adams inferred from magnetotelluric data. *Nature Geoscience* **2**, 785–789. <https://doi.org/10.1038/ngeo661>.
- Holland, T. & Blundy, J. (1994). Non-ideal interactions in calcic amphiboles and their bearing on amphibole-plagioclase thermometry. *Contributions to Mineralogy and Petrology* **116**, 433–447. <https://doi.org/10.1007/BF00310910>.
- Hollister, L. S., Grissom, G. C., Peters, E. K., Stowell, H. H. & Sisson, V. B. (1987). Confirmation of the empirical correlation of Al in hornblende with pressure of solidification of calc-alkaline plutons. *American Mineralogist* **72**, 231–239.
- Hopson, C. A. & Melson, W. G. (1990). Compositional trends and eruptive cycles at Mount St. Helens. *Geoscience Canada* **17**, 131–141.
- Humphreys, M. C., Blundy, J. D. & Sparks, R. S. J. (2006). Magma evolution and open-system processes at Shiveluch volcano: insights from phenocryst zoning. *Journal of Petrology* **47**, 2303–2334. <https://doi.org/10.1093/petrology/egl045>.
- Humphreys, M., Cooper, G. F., Zhang, J., Loewen, M., Kent, A. J. R., Macpherson, C. G. & Davidson, J. (2019). Unravelling the complexity of magma plumbing at Mount St. Helens: a new trace element partitioning scheme for amphibole. *Contributions to Mineralogy and Petrology* **174**, 9. <https://doi.org/10.1007/s00410-018-1543-5>.
- Jagoutz, O. E. (2010). Construction of the granitoid crust of an island arc. Part II: a quantitative petrogenetic model. *Contributions to Mineralogy and Petrology* **160**, 359–381. <https://doi.org/10.1007/s00410-009-0482-6>.

- Kent, A. J. (2014). Preferential eruption of andesitic magmas: implications for volcanic magma fluxes at convergent margins. *Geological Society, London, Special Publications* **385**, 257–280. <https://doi.org/10.1144/SP385.10>.
- Kiser, E., Palomeras, I., Levander, A., Zelt, C., Harder, S., Schmandt, B., Hansen, S., Creager, K. & Ulberg, C. (2016). Magma reservoirs from the upper crust to the Moho inferred from high-resolution Vp and Vs models beneath Mount St. Helens, Washington state, USA. *Geology* **44**, 411–414. <https://doi.org/10.1130/G37591.1>.
- Kiss, B., Harangi, S., Ntaflou, T., Mason, P. R. & Pál-Molnár, E. (2014). Amphibole perspective to unravel pre-eruptive processes and conditions in volcanic plumbing systems beneath intermediate arc volcanoes: a case study from Ciomadul volcano (SE Carpathians). *Contributions to Mineralogy and Petrology* **167**, 1–27. <https://doi.org/10.1007/s00410-014-0986-6>.
- Klaver, M., Matveev, S., Berndt, J., Lissenberg, C. J. & Vroon, P. Z. (2017). A mineral and cumulate perspective to magma differentiation at Nisyros volcano, Aegean arc. *Contributions to Mineralogy and Petrology* **172**, 95. <https://doi.org/10.1007/s00410-017-1414-5>.
- Leake, B. E., Wooley, A. R., Arps, C. E. S., Birch, W. D., Gilbert, M. C., Grice, J. D., Hawthorne, F. C., Kato, A., Kisch, H. J., Krivovichev, V. G., Linthout, K., Laird, J., Mandarino, J. A., Maresch, W. V., Nickel, E. H., Rock, N. M. S., Schumacher, J. C., Smith, D. C., Stephensen, N. C. N., Ungaretti, L., Whittaker, E. J. W. & Youzhi, G. (1997). Nomenclature of amphiboles: report of the Subcommittee on amphiboles of the international mineralogical association, commission on new minerals and mineral names. *American Mineralogist* **9**, 623–651. <https://doi.org/10.1127/ejm/9/3/0623>.
- Leeman, W. P. & Smith, D. R. (2018). The role of magma mixing, identification of mafic magma inputs, and structure of the underlying magmatic system at Mount St. Helens. *American Mineralogist* **103**(12), 1925–1944. <https://doi.org/10.2138/am-2018-6555>.
- Leeman, W. P., Smith, D. R., Hildreth, W., Palacz, Z. & Rogers, N. (1990). Compositional diversity of late Cenozoic basalts in a transect across the southern Washington cascades: implications for subduction zone magmatism. *Journal of Geophysical Research* **95**, 19561–19582. <https://doi.org/10.1029/JB095iB12p19561>.
- Rutherford, M. J. & Devine, J. D. (2008). Magmatic conditions and processes in the storage zone of the 2004–2006 Mount St. Helens dacite. In: Sherrod D. R., Scott W. E. & Stauffer P. H. (eds) *A volcano rekindled; the renewed eruption of Mount St. Helens, 2004–2006*. USGS Prof Pap 1750, pp.703–726.
- Melson, W. G. (1983). Monitoring the 1980–1982 eruptions of Mount St. Helens: compositions and abundances of glass. *Science* **221**, 1387–1391. <https://doi.org/10.1126/science.221.4618.1387>.
- Mullineaux, D. R. (1986). Summary of pre-1980 tephra-fall deposits erupted from Mount St. Helens, Washington state, USA. *Bulletin of Volcanology* **48**, 17–26. <https://doi.org/10.1007/BF01073510>.
- Mullineaux, D. R. (1996) *Pre-1980 tephra-fall deposits erupted from Mount St Helens*. Washington, USGS Prof Pap 1563.
- Mullineaux, D. R. & Crandell, D. R. (1981) The Eruptive History of Mount St. Helens. In: Lipman P. W. & Mullineaux D. R. (eds) *The 1980 Eruptions of Mount St. Helens*. Washington. U.S. Geological Survey Professional Paper 1250, pp.3–15.
- Müntener, O. & Ulmer, P. (2018). Arc crust formation and differentiation constrained by experimental petrology. *American Journal of Science* **318**, 64–89. <https://doi.org/10.2475/01.2018.04>.
- Pallister, J. S., Hoblitt, R. P., Crandell, D. R. & Mullineaux, D. R. (1992). Mount St. Helens a decade after the 1980 eruptions: magmatic models, chemical cycles, and a revised hazards assessment. *Bulletin of Volcanology* **54**, 126–146. <https://doi.org/10.1007/BF00278003>.
- Pallister, J. S., Clynne, M. A., Wright, H. M., Van Eaton, A. R., Vallance, J. W., Sherrod, D. R. & Kokelaar, B. P. (2017). Field-trip guide to Mount St. Helens, Washington—an overview of the eruptive history and petrology, tephra deposits, 1980 pyroclastic density current deposits, and the crater. USGS Sci Inv Rep 2017–5022-D.
- Pallister, J. S., Thornber, C. R., Cashman, K. V., Clynne, M. A., Lowers, H. A., Mandeville, C. W., Brownfield, I. K. & Meecker, G. P. (2008) Petrology of the 2004–2006 Mount St. Helens lava dome—implications for magmatic plumbing and eruption triggering. In: Sherrod D. R., Scott W. E. & Stauffer P. H. (eds) *A volcano rekindled: the renewed eruption of Mount St. Helens, 2004–2006*. USGS Prof Pap 1750, pp. 647–702.
- Pichavant, M., Martel, C., Bourdier, J.-L. & Scaillet, B. (2002). Physical conditions, structure, and dynamics of a zoned magma chamber: mount Pelée (Martinique, Lesser Antilles arc). *Journal of Geophysical Research* **107**. <https://doi.org/10.1029/2001JB000315>.
- Putirka, K. D. (2008). Thermometers and barometers for volcanic systems. *Reviews in Mineralogy and Geochemistry* **69**(1), 61–120. <https://doi.org/10.2138/rmg.2008.69.3>.
- Putirka, K. (2016). Amphibole thermometers and barometers for igneous systems and some implications for eruption mechanisms of felsic magmas at arc volcanoes. *American Mineralogist* **101**, 841–858. <https://doi.org/10.2138/am-2016-5506>.
- Ridolfi, F., Renzulli, A. & Puerini, M. (2010). Stability and chemical equilibrium of amphibole in calc-alkaline magmas: an overview, new thermobarometric formulations and application to subduction-related volcanoes. *Contributions to Mineralogy and Petrology* **160**, 45–66. <https://doi.org/10.1007/s00410-009-0465-7>.
- Riker, J., Blundy, J., Rust, A., Botcharnikov, R. & Humphreys, M. S. (2015). Experimental phase equilibria of a Mount St. Helens rhyodacite: a framework for interpreting crystallization paths in degassing silicic magmas. *Contributions to Mineralogy and Petrology* **170**, 1–22. <https://doi.org/10.1007/s00410-015-1160-5>.
- Rutherford, M. J. & Devine, J. D. (1988). The May 18, 1980, eruption of Mount St. Helens: stability and chemistry of amphibole in the magma chamber. *Journal of Geophysical Research* **93**, 11949–11959. <https://doi.org/10.1029/JB093iB10p11949>.
- Rutherford, M. J. & Devine, J. D. (2003). Magmatic conditions and magma ascent as indicated by hornblende phase equilibria and reactions in the 1995–2002 Soufriere Hills magma. *Journal of Petrology* **44**, 1433–1453. <https://doi.org/10.1093/petrology/44.8.1433>.
- Rutherford, M. J. & Hill, P. M. (1993). Magma ascent rate from amphibole breakdown: an experimental study applied to the 1980–1986 Mount St-Helens eruptions. *Journal of Geophysical Research* **98**(B11), 19667–19685. <https://doi.org/10.1029/93JB01613>.
- Sarna-Wojcicki, A., Meyer, C., Woodward, M. & Lamothe, P. (1981) Composition of air-fall ash erupted on May 18, May 25, June 12, July 22, and August 7. In: *The Eruption of Mount St. Helens*. Washington. USGS Prof Pap 1250, pp.667–681.
- Sauerzapf, U., Lattard, D., Burchard, M. & Engelmann, R. (2008). The Titanomagnetite–Ilmenite equilibrium: new experimental data and thermo-oxybarometric application to the crystallization of basic to intermediate rocks. *Journal of Petrology* **49**, 1161–1185. <https://doi.org/10.1093/petrology/egn021>.
- Scandone, R. & Malone, S. D. (1985). Magma supply, magma discharge and readjustment of the feeding system of Mount St. Helens during 1980. *Journal of Volcanology and Geothermal Research* **23**, 239–262. [https://doi.org/10.1016/0377-0273\(85\)90036-8](https://doi.org/10.1016/0377-0273(85)90036-8).
- Sisson, T. W., Ratajeski, K., Hankins, W. B. & Glazner, A. F. (2005). Voluminous granitic magmas from common basaltic sources. *Contributions to Mineralogy and Petrology* **148**, 635–661. <https://doi.org/10.1007/s00410-004-0632-9>.

- Smith, D. J. (2014). Clinopyroxene precursors to amphibole sponge in arc crust. *Nature Communications* **5**, 4329. <https://doi.org/10.1038/ncomms5329>.
- Smith, D. R. & Leeman, W. P. (1987). Petrogenesis of Mount St. Helens dacitic magmas. *Journal of Geophysical Research* **92**, 10313–10334. <https://doi.org/10.1029/JB092iB10p10313>.
- Smith, D. R. & Leeman, W. P. (1993). The origin of Mount St. Helens andesites. *Journal of Volcanology and Geothermal Research* **55**, 271–303. [https://doi.org/10.1016/0377-0273\(93\)90042-P](https://doi.org/10.1016/0377-0273(93)90042-P).
- Sun, S. S. & McDonough, W. F. (1989). Chemical and isotopic systematics of oceanic basalts: implications for mantle composition and processes. *Geological Society, London, Special Publications* **42**, 313–345. <https://doi.org/10.1144/GSL.SP.1989.042.01.19>.
- Thornber, C. R., Pallister, J. S., Lowers, H. A., Rowe, M. C., Mandeville, C. W. & Meeker, G. P. (2008). Chemistry, mineralogy, and petrology of amphibole in Mount St. Helens 2004–2006 Dacite, a volcano rekindled: the renewed eruption of Mount St. Helens, 2004–2006. U.S. Geological Survey Professional Paper 1750.
- Townsend, M., Huber, C., Degruyter, W. & Bachmann, O. (2019). Magma chamber growth during inter-caldera periods: insights from thermo-mechanical modeling with applications to Laguna del Maule, Campi Flegrei, Santorini, and Aso. *Geochemistry, Geophysics, Geosystems* **20**, 1574–1591. <https://doi.org/10.1029/2018GC008103>.
- Turner, S. J., Izbekov, P. & Langmuir, C. (2013). The magma plumbing system of Bezymianny volcano: insights from a 54 year time series of trace element whole-rock geochemistry and amphibole compositions. *Journal of Volcanology and Geothermal Research* **263**, 108–121. <https://doi.org/10.1016/j.jvolgeores.2012.12.014>.
- Walker, B. A., Bergantz, G. W., Otamendi, J. E., Ducea, M. N. & Cristofolini, E. A. (2015). A MASH zone revealed: the mafic complex of the Sierra Valle Fértil. *Journal of Petrology* **56**, 1863–1896. <https://doi.org/10.1093/petrology/egv057>.
- Wanke, M. (2019) *Petrological perspectives on the magmatic evolution of Mount St. Helens (Washington, US)*. Doctoral dissertation, ETH Zurich.
- Wanke, M., Clyne, M. A., von Quadt, A., Vennemann, T. W. & Bachmann, O. (2019a). Geochemical and petrological diversity of mafic magmas from Mount St. Helens. *Contributions to Mineralogy and Petrology* **174**, 10. <https://doi.org/10.1007/s00410-018-1544-4>.
- Wanke, M., Karakas, O. & Bachmann, O. (2019b). The genesis of arc dacites: the case of Mount St. Helens, WA. *Contributions to Mineralogy and Petrology* **174**, 7. <https://doi.org/10.1007/s00410-018-1542-6>.
- Waters, L. E. & Lange, R. A. (2015). An updated calibration of the plagioclase-liquid hygrometer-thermometer applicable to basalts through rhyolites. *American Mineralogist* **100**, 2172–2184. <https://doi.org/10.2138/am-2015-5232>.
- Zhang, J., Humphreys, M. C., Cooper, G. F., Davidson, J. P. & Macpherson, C. G. (2017). Magma mush chemistry at subduction zones, revealed by new melt major element inversion from calcic amphiboles. *American Mineralogist* **102**, 1353–1367. <https://doi.org/10.2138/am-2017-5928>.